DIRECT THROMBIN INHIBITION AND ATHEROSCLEROSIS

EVALUATING THE EFFECTS OF DIRECT THROMBIN INHIBITION IN A MOUSE MODEL OF SPONTANEOUS CORONARY ARTERY DISEASE AND MYOCARDIAL INFARCTION

By: LOUISE (YUN JOU) LEE, B.Sc. (Hons.)

A Thesis Submitted to the School of Graduate Studies in Partial Fulfilment of the Requirements for the Degree Master of Science

MASTER OF SCIENCE (2023)	McMaster University. Hamilton Ontario
TILE:	Evaluating the Effects of Direct Thrombin Inhibition in A Mouse Model of Spontaneous Coronary Artery Disease and Myocardial Infarction
AUTHOR:	Louise (Yun Jou) Lee, B.Sc. (Hons.) (University of Toronto-Mississauga)
SUPERVISOR:	Dr. Bernardo L. Trigatti
NUMBER OF PAGES:	xii, 54

ABSTRACT

Coronary heart disease involves atherosclerosis in coronary arteries, plaque rupture, and thrombosis, triggering myocardial infarction (MI). In commonly used mouse atherosclerosis models, plaques develop in the aorta, but not coronary arteries, and plaque rupture and thrombosis are rare. Mice lacking expression of the high-density lipoprotein receptor, scavenger receptor type B class I (SR-B1), and apolipoprotein E genes (apoE) are severely hypercholesterolemic, develop atherosclerosis spontaneously in coronary arteries, and exhibit MI and early death. This study aimed to better understand the involvement of thrombin by assessing fibrin deposition in coronary artery atherosclerosis development and MI in these mice. This was achieved by treating female and male SR-B1$^{ko/ko}$/apoE$^{ko/ko}$ mice with a diet supplemented with direct thrombin inhibitor, Dabigatran Etexilate (DE, 6 mg/g food, from 4-6 weeks of age). Clotting parameters (thrombin- antithrombin complex ELISA; thrombin generation assays) were measured using platelet-poor plasma. Atherosclerosis in the aortic sinus and coronary arteries was evaluated in cross-sections stained for lipids with oil red O and fibrin deposition in coronary arteries was evaluated by immunostaining. Myocardial fibrosis was detected by trichrome staining. Plasma cardiac Troponin-I and inflammatory cytokines IL-6, MCP-1, and TNF-α were measured by ELISA. The results showed that DE treatment reduced systemic inflammation, atherosclerotic plaque development in the aortic sinus and coronary arteries, and fibrin deposition in the atherosclerotic coronary arteries. It also reduced cardiomyocyte damage, but no changes were seen in cardiac fibrosis. In conclusion, while direct thrombin inhibition in a spontaneous coronary artery atherosclerosis murine model protected against some aspects of the disease development (coronary artery atherosclerosis, inflammation, myocardial damage

markers) it did not protect against others (myocardial fibrosis). Therefore, these results highlight the complexity of the involvement of thrombin in coronary heart disease.

ACKNOWLEDGMENTS

Where do I begin? My mind is still stuck on the day when I received my acceptance letter. It seems like just yesterday when I was completing all the onboard training to start my master's degree.

I want to begin by expressing my most sincere gratitude toward my supervisor Dr. Bernardo (Dino) Trigatti. He wasn't just my supervisor; he was someone who trusted me and took a chance on me. I wasn't a typical life science student and certainly did not have the research experience most of them do. All I had was a clear goal: to help people and a strong desire to achieve my goal by learning. However, Dr. Trigatti gave me the opportunity to believe in myself and show myself what I am capable of achieving. He gave me space when I needed it and held me accountable when I strayed away. I am truly lucky to be one of his students and I am forever grateful for his presence, guidance, and support throughout my degree. I would also like to extend my gratitude towards my committee members, Dr. William Sheffield, and Dr. Jeffrey Weitz, both of whom have been extremely patient and supportive in my journey. My research would not have been possible without their knowledge and expertise.

To my amazing and intelligent lab mates at the Trigatti lab, thank you for sharing this journey with me. Thank you all for being so selfless with your time and knowledge, and always ready and willing to help me whenever I needed support. Ting Xiong, thank you for being such a great mentor and teaching me all the procedures related to mouse work and atherosclerosis measurements. Thank you for being so patient with my questions and taking time out of your

own experiments to help me. Sumayyah Sokeechand, thank you for being my listening ear and getting me through a tough day. You lifted me when my spirits were down. You showed me such tender care by always prioritizing my well-being before yours. You made such an impact on my life that goes beyond this degree, and for that, I am so thankful to have met you. Last but not least, I would like to give a huge thank you to Rida Malik from the Weitz Lab. Thank you for taking care of my research like it was your own. You were never shy to share your knowledge and always took the time to troubleshoot with me when my experiments fell short. Without you, my research would not have been possible and for that, I appreciate you immensely.

To my loving parents, nothing I say or do will ever amount to the love and support you have given me. You have always given me the freedom to do whatever my heart desired and supported every decision I made. You have taught me to dream big, work hard, and love unconditionally. Thank you for giving me a life of opportunities, I owe everything to both of you.

Lastly, I started this degree in hopes to help people, and with the countless hours of work in the lab I hope my work can shed some light on coronary artery disease and more importantly, improve the lives of those who suffer from it.

TABLE CONTENTS

LIST OF FIGURES

LIST OF ABBRIVIATIONS

apoE	apolipoprotein E
ANOVA	analysis of variance
APC	activated protein C
CA	coronary artery
cTnI	cardiac troponin I
DTI	direct thrombin inhibitor
DE	dabigatran etexilate
DOAC	direct oral anticoagulant
dKO	double knockout
ECM	extracellular matrix
ELISA	enzyme-linked immunosorbent assay
ERK	extracellular signal-regulated kinase
EFGR	epidermal growth factor receptor
FDA	food and drug administration
HDL	high-density lipoprotein
IL-6	interleukin-6
ICAM-1	intercellular adhesion molecule-1
IF	immunofluorescent
LMWH	low molecular weight heparin
LDL	low-density lipoprotein
LDLR	low-density lipoprotein receptor
mAb	monoclonal Antibody
MCP-1	monocyte chemoattractant protein-1
MOM	mouse on mouse
MMP	matrix metalloproteinase
NO	nitric oxide

Ox-LDL	oxide low-density lipoprotein
PDGF	platelet-derived growth factor
PAR-1	protease-activated receptor-1
SR-B1	scavenger receptor class B type I
SMC	smooth muscle cell
SKO	single knockout
TF	tissue factor
TAT	thrombin-antithrombin complex
TNF-α	tumor necrosis factor-alpha
TGA	thrombin generation assay
VCAM-1	vascular adhesion molecule-1
VKA	vitamin K antagonist
VLDL	very low-density lipoprotein

DECLARATION OF ACADEMIC ACHIEVEMENT

All work has been performed by Louise (Yun Jou) Lee.

Chapter 1: Introduction

In Canada, heart disease is the second leading cause of death with ischemic heart disease representing the most common form[1,2]. Ischemic heart disease is a collective term given to heart diseases that result in a reduced blood flow to the heart due to the narrowing of the arteries supplying the heart[2] . This is also known as coronary heart disease. Coronary heart disease is a consequence of atherosclerotic plaque development in the coronary arteries[3]. Atherosclerosis is a chronic inflammatory disease characterized by the accumulation of lipids and the formation of plaques[3]. Over time, the development of plaques can narrow the arteries, or in advanced stages, rupture, and lead to the formation of blood clots[3]. In either case, the development of plaque poses a serious health risk as it can lead to blockage of blood flow which is essential for oxygen delivery.

1.1 Atherosclerosis Development

The development of atherosclerosis can be categorized into three stages, fatty streak, plaque progression, and plaque disruption[4]. In the early stage, the fatty streak is characterized by yellow discoloration due to a build-up of cholesterol on the inner surface of the artery wall, and crucial to this stage is the dysfunction of the endothelium[4]. This can be a result of reduced Nitric Oxide (NO) bioavailability or disruption of hemodynamic forces (i.e., low shear stress) in the endothelium[4]. NO is synthesized by endothelial cells and promotes endothelium-dependent vasodilation. It is considered an athero-protective molecule because it reduces platelet aggregation, tissue oxidation, and inflammation. However, NO production is reduced in hyperlipidemic conditions which leads to increases in oxidative stress and proinflammatory responses. Hemodynamic forces in the vessel wall (shear stress) also play a critical role in endothelial dysfunction. Areas along the vessel wall that bifurcates, or branches (low shear

stress) are more susceptible to the accumulation of Low-Density Lipoproteins (LDLs) and a favorable environment for plaque localization due to the disturbances in blood flow. Ultimately, these insults to the endothelium increase its permeability and allow for the transcytosis of LDLs to occur. When LDLs are transported from the lumen to the subendothelial space it undergoes chemical oxidation. These oxidized LDLs (ox-LDLs) are pro-inflammatory and broadly speaking, contain protein components that are structurally modified by aldehyde products to produce a net negative charge that is essential for the interaction and uptake by macrophages[5]. In addition, ox-LDLs can initiate inflammatory signaling, leading to the activation of adhesion molecules such as P -selectin, E-selectin, Intercellular Adhesion Molecule 1 (ICAM-1), and Vascular Adhesion Molecule 1 (VCAM-1)[5]. These adhesion molecules are essential for leukocyte recruitment. In the early stages of the recruitment, P-selectin and E-selectin participate in rolling adhesion, allowing leukocytes to transiently bind to the endothelial surface, while in the later stage, ICAM-1 and VCAM-1 participate in tightening and firming the adhesion to allow for the transmigration of leukocytes into the intima[6]. In the context of atherosclerosis, monocytes are important leukocytes that transmigrate into the intima and mature into phagocytic macrophages with the upregulation of scavenger receptors to remove ox-LDLs[7]. Once these macrophages ingest ox-LDLs they become foam cells and the accumulation of lipid-engorged foam cells in the artery wall is the hallmark of atherosclerosis and is thought to drive plaque growth[3,4,7]. During the plaque progression stage, there is a constant turnover of macrophages to promote the resolution of inflammatory responses. While newly recruited macrophages contribute to the accumulation of foam cells, older foam cells undergo cell death forming the necrotic core commonly associated with plaques which further the inflammatory response[3,4]. Furthermore, the progression of plaques is enhanced by the proliferation of Smooth Muscle Cells

(SMCs) stimulated by growth factors such as Platelet-Derived Growth Factor (PDGF) released from foam cells, activated platelets, and endothelial cells[4,8]. The migration of SMCs to the intima forms the fibrous cap of the plaque and acts as a protective layer to prevent plaques from rupturing and spilling their content into the bloodstream. In addition, surrounding the SMCs is the Extracellular Matrix (ECM). The ECM composes a mixture of collagen, elastin, glycoproteins, and proteoglycans that are vital for providing structural integrity to various organs, including the heart and the vascular network[8]. The ECM helps reinforce the stability of the fibrous cap of the plaque, however, in atherosclerosis, the regulation of ECM is altered[8,9]. ECM is regulated by Matrix Metalloproteinase (MMPs) and their tissue inhibitors. MMPs are produced by macrophages, and they are capable of digesting the ECM which weakens the fibrous cap and contributes to the instability of the plaque[9]. The final stage of atherosclerosis development is marked by the rupturing of unstable plaques[4]. This rupture leads to highly prothrombotic plaque material spilling into the lumen and triggering the activation of the coagulation pathway[3,4,10] (Refer to figure 1).

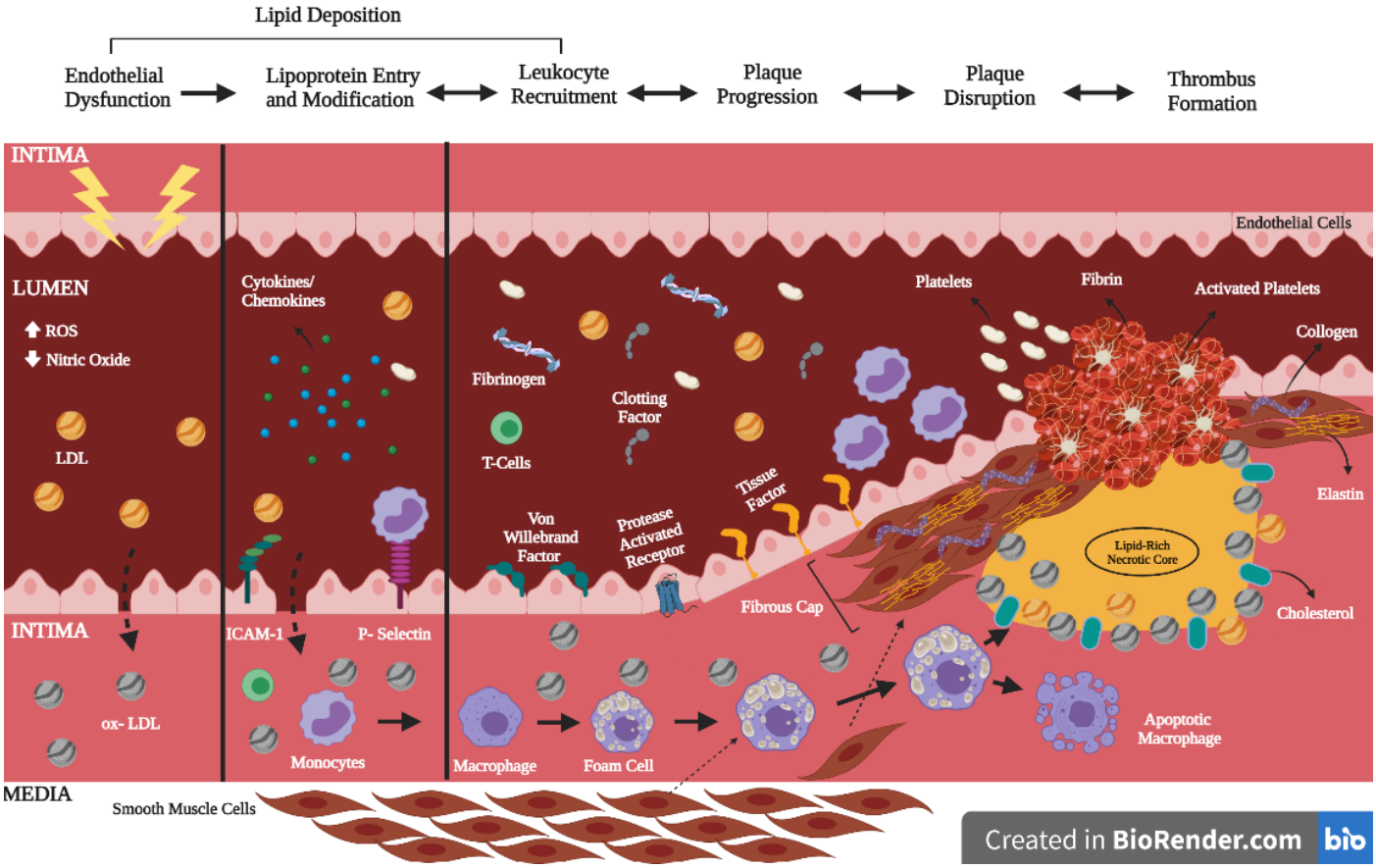

Figure 1: Atherosclerosis Development[4]. There are three stages, lipid deposition, plaque progression, and plaque disruption that capture the progression of atherosclerosis development. Fatty streak marks the beginning of plaque development and begins with endothelium dysfunction due to chemical or physical irritations. This leads to an increase in the permeability of the endothelium allowing the entry of LDLs into the intima and undergo chemical modification to form highly inflammatory ox-LDLs. Furthermore, these irritations activate adhesion molecules on the endothelium triggering an inflammatory response. These inflammatory responses lead to the recruitment of leukocytes, particularly monocytes/macrophages. Plaque progression is marked by the continuous ingestion of ox-LDLs by macrophages as an attempt to reduce inflammation. These macrophages become foam cells. The accumulation of foam cells stimulates smooth muscle cell migration and proliferation and contribute to the growth of the plaque. Over time, degradation enzymes such as MMPs render the growing plaque unstable and lead to the final stage of plaque rupture and thrombus formation.

1.2 Coagulation Pathways

The coagulation pathway is a cascade of events that leads to the reduction of blood loss at the site of injury by forming clots, a process known as hemostasis[11,12]. There are three pathways, the intrinsic, extrinsic, and common pathways, and each pathway consists of different clotting factors that aid in the final conversion of soluble fibrinogen into insoluble fibrin clot[11,12]. Most of the clotting factors are produced in the liver and circulate in the blood as inactive forms called zymogens, and upon activation, they become serine proteases which act as catalysts to cleave downstream zymogens[11,12]. The intrinsic pathway is activated when FXII comes in contact with negatively charged molecules or surfaces, initiating a sequential activation of FXI and FIX, and resulting in the formation of FIXa-FVIIIa complex; whereas the extrinsic pathway is activated when there is injury or trauma to the endothelium resulting in the release of TF[11–13]. The TF then binds to FVIIa forming a TF-FVIIa complex[12,13]. Both the intrinsic FIXa-FVIIIa complex and the extrinsic TF-FVIIa complex then merge into the common pathway and activate FX, then thrombin[12,13]. The final stage of coagulation is marked by the conversion of fibrinogen to fibrin. Fibrinogen is a glycoprotein complex synthesized in the liver[12,14]. Once thrombin converts fibrinogen to fibrin, fibrin polymerization processes such as elongation, lateral aggregation, and cross-linking can occur to form the final product of an insoluble fibrin clot[15]. While the waterfall/cascade model of the coagulation pathway is useful in understanding how each clotting factor relates to one another and the steps required for fibrin clot formation[12], it is not a comprehensive view of the coagulation process at a physiological level in the vasculature[16]. The cell-based model of the coagulation pathway considers the importance of cells' role in the formation of a fibrin clot[16]. Specifically, there are three phases, initiation, amplification, and propagation involved in the formation of a fibrin clot. The initiation phase is when TF-bearing

cells such as macrophages expose TF providing a surface in which circulating clotting factors can assemble upon[16]. The amplification phase occurs when small amounts of thrombin generated from the extrinsic pathway activate clotting factors in the intrinsic pathway leading to a burst of thrombin generation which leads to the propagation phase where a stabilized fibrin clot is formed (Refer to Figure 2).

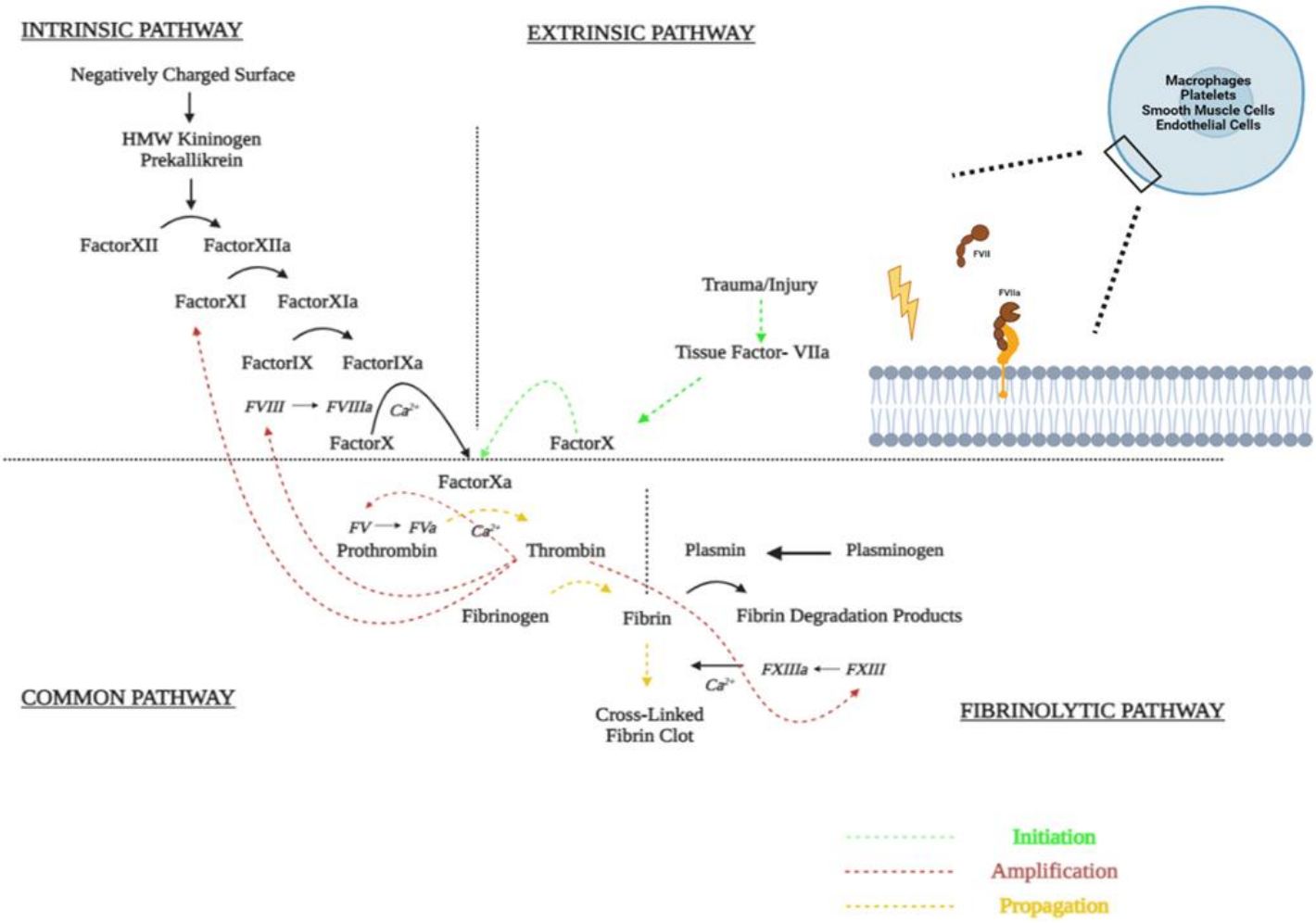

Figure 2: Coagulation Pathways[12,16]. This figure illustrates key players in the coagulation and fibrinolytic pathways. The coagulation pathway is subdivided into three pathways, intrinsic, extrinsic, and common pathways. The intrinsic pathway is activated when it is in contact with negatively charged molecules or surfaces, whereas the extrinsic pathway is activated when there is physical injury/trauma to the blood vessel. Both the intrinsic and extrinsic pathway merge into the common pathway leading to the final product of fibrin clot formation. The fibrinolytic pathway is activated upon the formation of fibrin clots and is responsible for the degradation of them. Furthermore, cells are important in facilitating the activation of the coagulation pathway. According to the cell-based model of coagulation[16], the Initiation involves cells releasing Tissue Factor to generate limited amounts of thrombin (green dotted line). The Amplification stage occurs when the intrinsic pathway is activated creating a positive feedback loop for greater amounts of thrombin generation (red dotted line). Finally, the Propagation stage involves fibrin clot formation upon continuous stimulation of both intrinsic and extrinsic pathways (yellow dotted line). *Created in BioRender.com.*

1.3 Coagulation Pathways and Atherosclerosis Development

Unlike the inflammatory pathway, our understanding of the roles of the coagulation pathway in the development of atherosclerosis is limited. Atherothrombosis occurs when the plaque ruptures leading to the formation of a superimposed thrombus, however, thrombus formation can also take place within a growing plaque[17]. This is usually a result of angiogenesis-related neo-vessel formation within the plaque and these vessels are said to be leaky and prone to rupture, exposing blood to the highly thrombogenic plaque content leading to microthrombi formation[18]. In atherothrombosis, exposure of TF on ruptured endothelium, as well as monocytes/ macrophages in plaque lesions, serve as an initiator of the extrinsic pathway[19–21]. In addition, the formation of the TF-FVIIa complex can also stimulate the activation of the intrinsic pathway through activating FIX, thereby amplifying the production of thrombin and subsequently fibrin clot formation[19–21]. Many cells are involved in atherosclerosis development that is also TF-bearing cells such as smooth muscle cells, macrophages, platelets, and endothelial cells[22]. These cells are capable of activating the coagulation pathway through exposing TF upon stimulation which allows circulating clotting factors to assemble on and form a fibrin clot[16,22]. While TF is crucial in the activation of the coagulation pathway in atherosclerosis development, other coagulation proteins such as thrombin have also been implicated in affecting the thrombogenicity of plaque development. Therefore, the interplay between the coagulation pathway and inflammatory pathway suggests an important role in determining the course of atherosclerosis development.

1.4 Thrombin

Thrombin is a functionally diverse protein that affects both the coagulation and inflammatory pathways thus playing a particularly important role in the development of

atherosclerosis[21,23]. In the coagulation pathway, thrombin exhibits both procoagulant and anticoagulant properties[23]. The procoagulant property is attributed to thrombin's ability to activate platelets leading to increased platelet aggregation and adhesion, as well as its ability to activate other clotting factors and being responsible for converting fibrinogen to fibrin[23]. In contrast, when thrombin binds to thrombomodulin on endothelial cells, it leads to the conversion of protein C to activated protein C (APC). APC inhibits thrombin generation by inactivating FVa and FVIIIa resulting in anti-coagulant responses. In the inflammatory pathway, thrombin's proinflammatory effects are mediated by G-protein-coupled receptors (GPCR), and protease-activated receptors (PARs)[23]. There are four members of the PAR family (PAR1-4), and thrombin activates PAR-1, PAR-3, and PAR-4[24,25]. It is important to note that there are differences in the expression of PAR on cells between humans and mice. For example, human platelets express PAR-1 and PAR-4, whereas mouse platelets express PAR-3 and PAR-4[25]. Nevertheless, PAR-1 is a potent substrate for thrombin and is located on most cells essential in atherosclerosis development such as endothelial cells, platelets, macrophages, and vascular smooth muscle cells[23–25]. When activated it leads to growth, differentiation, and proliferation of cells[23]. Consequently, thrombin promotes both atherogenic and thrombogenic development in plaques in atherosclerosis. The functionally diverse nature of thrombin makes it a desirable target for intervention. There are two categories of thrombin inhibitors, direct and indirect[26]. Structurally, thrombin has three domains in which thrombin-inhibiting drugs can bind, the catalytic site, and two exosites. Exosite I is the binding site for fibrinogen while exosite II is the binding site for heparin[27].

Indirect thrombin inhibitors such as unfractionated heparin and Low-Molecular-Weight Heparin (LMWH) require the presence of a cofactor, antithrombin[27]. Antithrombin binds to the

active site on thrombin while heparin binds to antithrombin and Exosite II on thrombin, simultaneously, resulting in the formation of a ternary complex of heparin-thrombin-antithrombin[27]. However, heparin can also bind simultaneously to fibrin and thrombin, occupying both the exosites and creating a fibrin-heparin-thrombin complex while leaving the active site exposed[27]. In this case, heparin enhances thrombin's affinity for fibrin leading to an increase in thrombin-bound fibrin concentration and ultimately fibrin clot formation[27].

On the other hand, direct thrombin inhibitors (DTIs) not only do not require the assistance of a cofactor and bind directly to the active site and exosite I of thrombin but also bind to free and clot-bound thrombin[26,27]. One such DTI of interest is Dabigatran, sold as a prodrug, Dabigatran Etexilate (DE)[28]. Dabigatran's inhibition of thrombin is rapid, competitive (*Ki*= 4.5 nM), and reversible with high selectivity compared to other thrombin inhibitors[29]. DE is classified as Direct Oral Anticoagulant (DOAC). Many DOACs are gaining considerable attention because they have shown superiority or noninferiority to the current standard of care anticoagulants such as Warfarin, a Vitamin K Antagonist (VKA), and LMWH[28]. In addition, DOACs have many advantages compared to VKA such as fewer monitoring requirements, less frequent follow-ups, more immediate drug onset and offset, and fewer drug and food interactions[28]. DE is a prodrug which is administered orally and converted to the active form, Dabigatran, in the liver[30]. It has an absolute bioavailability of 6.5% and is measured to be 2-fold less potent in mice compared to human[29]. The serum half-life is 12 to 17 hours and 80% of the given dose is excreted by the kidneys [31]. The FDA-approved indications for DE prescribing include stroke prevention for non-valvular atrial fibrillation, treatment and prevention of recurrent deep vein thrombosis and pulmonary embolism, and prevention of thromboembolism after total hip replacement[28].

In animal studies, apoE$^{ko/ko}$ (SKO) mice treated with DE showed reduced aortic sinus atherosclerosis, macrophage infiltration and accumulation, and thrombin-mediated platelet aggregation[32–35]. In addition, DE treatment also improved endothelial function[32–34] and has been shown to change plaque composition associated with markers of plaque stabilization by thickening the fibrous cap through smooth muscle cell proliferation and collagen and elastin deposition[35]. In human studies, there have been many clinical trials undertaken to examine the long-term efficacy and safety of DE in relation to other DOACs[36], existing standard of care (i.e., warfarin)[31,37,38], different indications (i.e., coronary artery disease)[39,40], and combined therapies (i.e., dual anti-platelet therapy plus antithrombotic therapy)[38–40]. Perhaps, the most problematic aspect of DE is its association with an increased risk of myocardial infarction compared to Warfarin [31,37,41]. Furthermore, the results of combined therapy of DE in addition to dual platelet therapy for the treatment of atrial fibrillation comorbid with coronary artery disease have been conflicting. This is mainly because compound cardiovascular diseases usually require triple antithrombotic therapy, however, with the addition of an antithrombotic therapy there is an increased risk of bleeding, while the risk of thrombosis remains unclear[28,39,40]. Therefore, the verdict on DE's efficacy and safety is still out for debate and there are still many aspects and conditions that need to be considered and especially in the case of coronary artery disease.

1.5 Mouse Models in Atherosclerosis

In general, animal models in atherosclerosis are based on accelerated plaque formation as a result of either a cholesterol-rich/western-type diet, genetic manipulation involved in cholesterol metabolism, or the introduction of additional risk factors for atherosclerosis such as diabetes[42,43]. While various animal species have been utilized in studying atherosclerosis, mice have been the preferred species because of their well-studied genetic profile[42]. However, mice are resistant to

developing atherosclerosis, thus to utilize them in research genetic manipulation of their lipid metabolism is required[42]. The most common genetic manipulations in an atherosclerotic mouse model are the knockout of apolipoprotein E (apoE) and Low-Density Lipoprotein Receptor (LDLR) genes. apoE is a glycoprotein that functions as a ligand for receptors that clear chylomicrons and Very-Low Density Lipoprotein (VLDL), and by knocking out the apoE genes ($apoE^{ko/ko}$), plasma total cholesterol level increases[42]. Similarly, since mice have higher levels of High-Density Lipoprotein (HDL) and lower levels of LDLs, by knocking out LDLR ($LDLR^{ko/ko}$), researchers have significantly increased the plasma LDL cholesterol levels[42].

The development of atherosclerosis can be accelerated when combining genetic manipulations with high-fat and high-cholesterol diets[42,43]. However, these mice usually develop atherosclerosis in the aortic sinus and not in the coronary arteries, in addition, spontaneous plaque rupture and/or thrombotic complications rarely occur at this site, thus LDLR and apoE knockout mice models are not very useful in understanding coronary atherothrombosis and myocardial infarction[42].

However, coronary artery atherosclerosis and myocardial infarction were observed in mice in which both the Scavenger Receptor Class B Type I (SR-B1) and apoE genes were knocked out[44]. SR-B1 is an important receptor for HDL and reduces circulating lipids by facilitating the selective delivery of cholesterol from HDL to steroidogenic tissues and the liver for excretion into bile and feces[43]. A previous study by Braun et al. (2002) found that on a standard laboratory diet, $SR\text{-}B1^{ko/ko}/apoE^{ko/ko}$ (dKO) mice showed signs of coronary artery disease, including occlusive coronary atherosclerosis, spontaneous myocardial infarction, and cardiac hypertrophy and dysfunction[44]. Consequently, these mice had a significantly reduced lifespan with a reported average premature death at 6 weeks of age[44]. Intriguingly, that study reported the detection of

fibrin deposition in atherosclerotic coronary arteries of dKO mice, suggesting the involvement of the coagulation pathway in coronary artery disease. However, the extent of fibrin deposition among atherosclerotic coronary arteries and the importance of fibrin deposition for coronary artery disease and myocardial infarction development were not tested.[44]. Furthermore, the role of the coagulation pathway in the development of atherosclerosis was further demonstrated by platelet activation detected in other similar coronary artery atherosclerosis studies utilizing the dKO mouse model[44,45] (Refer to Figure 3). Therefore, the unique nature of the coronary artery disease development in the dKO mice and the potential involvement of fibrin deposition in atherosclerotic coronary arteries in coronary artery disease development suggest that this mouse model may be a useful preclinical model for probing the impacts of direct thrombin inhibition on coronary artery disease, coronary atherothrombosis, and myocardial fibrosis.

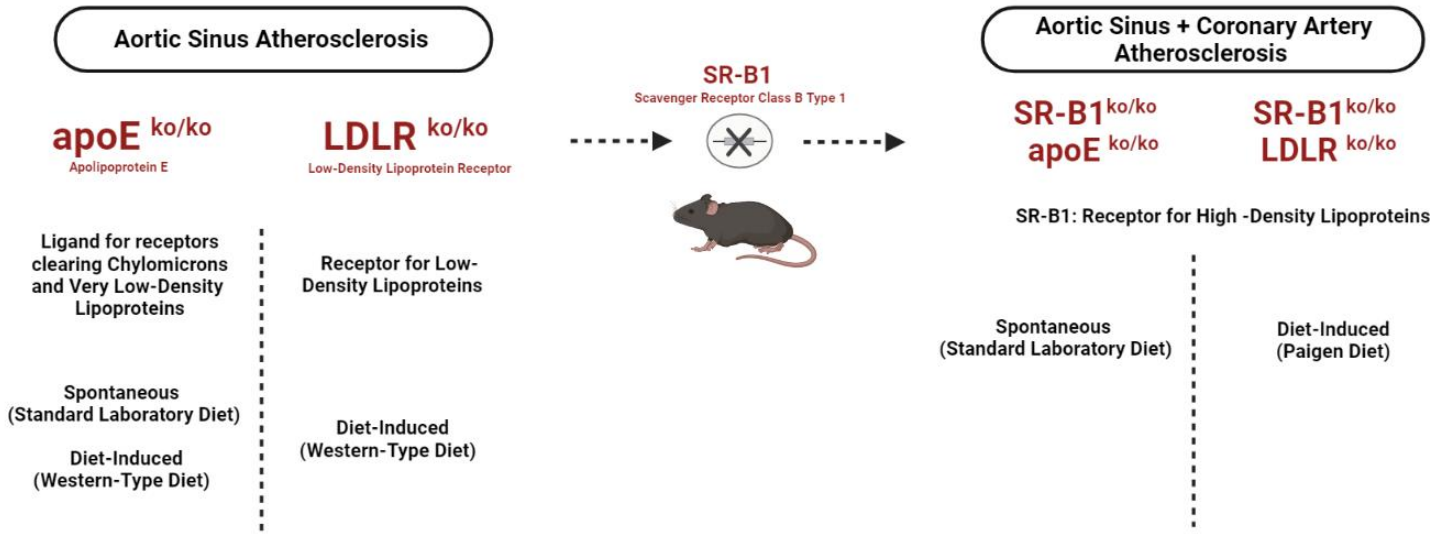

Figure 3: Mouse Models in Atherosclerosis[42,43]. This figure illustrates key mouse models in studying atherosclerosis. Most commonly, studies utilize apoE$^{ko/ko}$ or LDLR$^{ko/ko}$ to study atherosclerosis development. These mouse models develop accelerated atherosclerosis in the aortic sinus while on western-type diet, though apoE$^{ko/ko}$ can develop atherosclerosis spontaneously, it would require an extended period. By additionally knocking out the gene SR-B1 these mice develop coronary artery atherosclerosis in addition to aortic sinus atherosclerosis. The major difference is that SR-B1$^{ko/ko}$/apoE$^{ko/ko}$ develops atherosclerosis spontaneously on standard laboratory diet while SR-B1$^{ko/ko}$/LDLR$^{ko/ko}$ mice develops it on a Paigen diet. *Created in BioRender.com.*

Chapter 2: Hypothesis and Objectives

2.1 Hypothesis

The inhibition of thrombin by dabigatran will reduce fibrin deposition and plaque development in the coronary arteries of SR-B1$^{ko/ko}$ apoE $^{ko/ko}$ mice.

2.2 Objectives

1. To characterize the time course development of atherosclerosis and fibrin deposition in the aortic sinus and coronary arteries in SR-B1$^{ko/ko}$ apoE $^{ko/ko}$ mice.

2. To investigate the effects of direct thrombin inhibition on coronary artery atherosclerosis, fibrin deposition, and myocardial infarction in SR-B1$^{ko/ko}$ apoE $^{ko/ko}$ mice.

Chapter 3: Methods and Materials

3.1 Mice

All procedures involving mice were approved by the Animal Research Ethics Board of McMaster University and followed the guidelines of the Canadian Council on Animal Care. Mice were bred and housed in the David Braley Research Institute animal facility in ventilated cages with automatic watering and had free access to either standard normal laboratory diet in pellets (Catalog # Teklad – 2918-032222M) or powder (Catalog # Teklad – 2918M.CS) containing 18% protein, 5% fat, and 5% fiber (Teklad Global, Envigo, Mississauga, ON, Canada). dKO mice were produced by mating SR-B1$^{wt/ko}$ apoE$^{ko/ko}$ (mixed C57BL/6J and 129Sv genetic background) mice derived from founders originally provided by Monty Krieger, Massachusetts Institute of Technology, Cambridge, USA. Genotyping was carried out by PCR on DNA isolated from tail biopsies collected at weaning (3 weeks of age).

3.2 Dabigatran Etexilate (DE) Treatment

0.6g of DE (Toronto Research Chemicals, Toronto, ON, Canada, catalog # D100140) was mixed with 100g of standard normal laboratory diet in powder (Takled Global, Envigo, Mississauga, ON, Canada, catalog # Teklad – 2918M.CS). Food was mixed with autoclaved water and placed in food cups for feeding. Treatment began when dKO mice were 4 weeks old and continued for two weeks. Each cage housed two mice, and they were given two cups of food per day.

3.3 Euthanasia and Heart Collection

Mice were anesthetized with isoflurane/O_2. Hearts were perfused in situ with phosphate-buffered saline containing 10 U of heparin/ml and stored in Shandon Cryomatrix (Fisher Scientific, Ottawa, ON, Canada) at -80°C.

3.4 Plasma Blood Collection

Blood was collected through the Inferior Vena Cava using a 3ml syringe with a 23G x 1″ gauge needle that was loaded with 10µl buffered citrate/ 1ml blood. To collect platelet-poor plasma, blood was centrifuged twice at 8000 rpm for 10 minutes and the supernatant was collected, aliquoted, and stored at -80º C.

3.5 Diluted Thrombin Time

Platelet-poor plasma was first diluted to 1:8 with HEPES-buffered saline (20 mM HEPES and 150 mM NaCl). Then, in a clear round-bottom 96-well plate 50 µl of the diluted plasma was mixed with 100 µl of normal human plasma and incubated for 60s at 37º C. Finally, 100 µl of substrate buffer (2 nM human alpha thrombin (Enzyme Research Laboratories Inc., Indiana, United States, catalog # HT 10002a and 4 mM $CaCl_2$) was added to the mixed plasmas and read at an absorbance of 405 nm for 90 minutes at 37º C using Molecular Devices ThermoMax Microplate Reader. To establish the standard curve, plasma, and substrate buffer were mixed with varying dabigatran concentrations (0-500 ng/ml). This resulted in various clotting times and the corresponding dabigatran concentration was used to generate a standard curve. The concentration of dabigatran in the unknown plasma was determined by extrapolating the clotting

time along the standard curve. The R- squared value of the standard curve was 0.96 (Refer to Figure 7A).

3.6 Enzyme-Linked Immunosorbent Assays (ELISAs)

Thrombin-Antithrombin (TAT) ELISA kit was purchased from Affinity Biologicals Inc. (Ancaster ON, Canada, catalog # TAT-EIA). Stock capture antibody contained 0.5 ml of polyclonal affinity purified anti-thrombin antibody and was diluted with coating buffer (50 mM carbonate) to 1:200. Similarly, stock detecting antibody contained 0.5 ml of peroxidase-conjugated affinity-purified polyclonal anti-Antithrombin III antibody and was diluted with conjugated diluent to 1:200. Platelet-poor plasma was diluted with Sample Diluent to 1:5. OPD (o-phenylenediamine dihydrochloride, 5mg) substrate tablets (Sigma- Aldrich, Oakville, ON, Canada, catalog # P6912-50TAB) were dissolved in citrate-phosphate buffer (0.1 M sodium phosphate and 0.02 M citric acid, pH 5.0) with 12 µl of 30% hydrogen peroxide and added to each plate at the end. At any given stage, the reaction volume was 100 µl. A high-binding ELISA 96-well plate (Corning Inc. New York, United States) was used. Each plate was given 5 minutes for color development and the reaction was stopped by adding 50 µl of 2.5 M sulfuric acid. The plates were read using Molecular Devices ThermoMax Microplate Reader at an absorbance of 490 nm.

IL-6 (catalog # 431304), TNF-α (catalog # 430904), and MCP-1 (catalog # 432704) ELISA kits were purchased from BioLegend (California, United States). Stock capture antibodies IL-6 (mouse anti-rat monoclonal antibody), TNF-α (mouse anti-Armenian hamster monoclonal antibody), and MCP-1 (mouse anti-Armenian hamster monoclonal antibody) were

diluted with coating buffer to 1:200. Platelet-poor plasma was diluted to 1:4 with assay diluent. Stock detection antibodies IL-6 (rat anti-mouse biotinylated monoclonal antibody), TNF-α (goat anti-mouse biotinylated polyclonal antibody), and MCP-1 (Armenian hamster anti-mouse biotinylated monoclonal antibody) were diluted to 1:200 with assay diluent. Avidin-HRP was diluted to 1:1000 with assay diluent. High binding ELISA 96-well plates (Corning Inc. New York, United States). At any given stage, the reaction volume was 100 µl. Equal volumes of TMB (3,3',5,5'-Tetramethylbenzidine) substrates were added to each well and given 15 minutes for color development. The reaction was stopped by adding 50 µl of 1 M sulfuric acid. The plates were read using Molecular Devices ThermoMax Microplate Reader at an absorbance of 450 nm.

Mouse Cardiac Troponin- I (cTnI) ELISA kit was purchased from Life Diagnostics Inc. (Pennsylvania, United States, catalog # CTNI-HSP). Platelet-poor plasma was diluted to 1:2 with plasma diluent. Each well was given 20 minutes for color development and the reaction was stopped by adding 50 µl of stop solution. The plates were read using Molecular Devices ThermoMax Microplate Reader at an endpoint absorbance of 450 nm.

3.7 Thrombin Generation Assay (TGA)

Platelet-poor plasma (40 µl) was mixed with 10 µl of Activated Partial Thromboplastin (Instrumentation Laboratories, Massachusetts, United States, catalog # 0008468710) and 50 µl of substrate buffer. The substrate buffer consisted of 260 nM of $CaCl_2$, 20 nM of HEPES, and 20 nM fluorogenic substrate (Z-Gly-Gly-Arg-AMC) (Bachem Americas, Inc. United States, catalog #4002155.0025). Each mixture was dispensed in an opaque round bottom 96-well plate and read at 37º C for 90 minutes between 360 nm and 460 nm wavelengths using Molecular Devices

ThermoMax Microplate Reader. The raw values generated were transferred to TECHNOTHROMBIN® TGA Evaluation Software (Technoclone Herstellung von Diagnostika und Arzneimitteln GmbH, Austria) for analysis.

3.8 Aortic Sinus Atherosclerosis

Transverse cryosections (10 µm) were obtained using Shandon Cryotome Cryostat (Thermo Fisher Scientific, Ottawa, ON, Canada). They were stained for lipids with Oil red O (Thermo Fisher Scientific, Ottawa, ON, Canada, catalog # AAA1298914) and counterstained for nuclei with Hematoxylin (Sigma- Aldrich, Oakville, ON, Canada, catalog # MHS80-2.5L). The aortic sinus atherosclerotic plaque area within all three leaflets at different positions (0 µm, 100 µm, 200 µm, 300 µm, or 400 µm, refer to figure 4) was quantified using Axiovision software. The atherosclerotic plaque volume was calculated as the area under the curve of plaque area versus distance 0 µm to 400 µm. Bright-field microscopy with 5x magnification was used to capture all images (Zeiss Axiovert 200M Fluorescence Microscope).

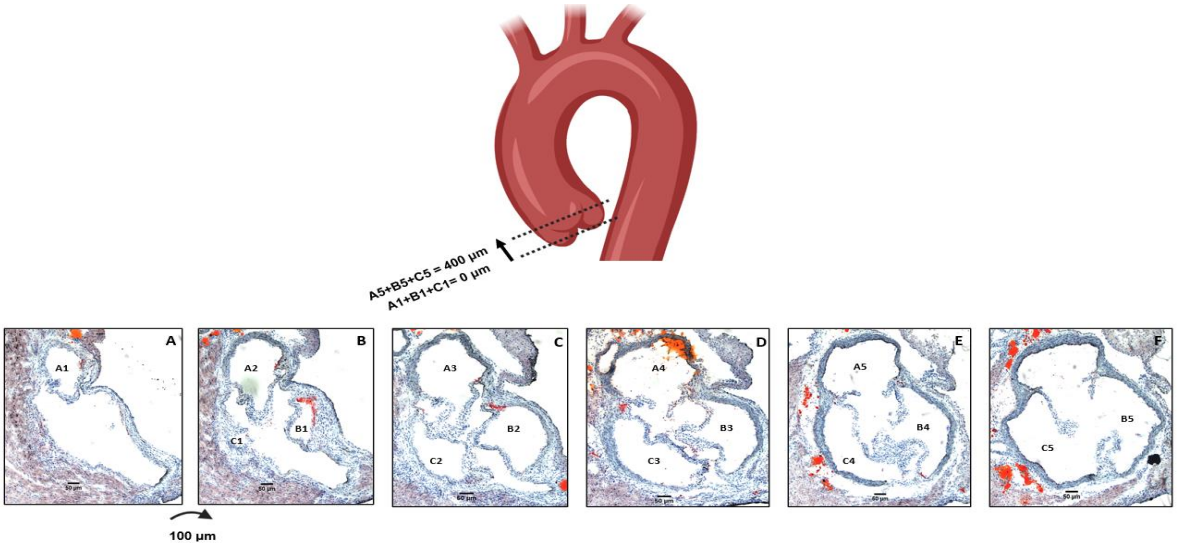

Figure 4: Aortic Sinus Section and Quantification Figures A-F show the appearance to the disappearance of all three aortic sinus valve leaflets, respectively. Each figure is 100 µm apart and each aortic sinus valve leaflet is labeled either A, B, or C and quantified for 5 sections (0 µm to 400 µm).

3.9 Coronary Artery Atherosclerosis

Transverse cryosections (10 μm) were obtained using Shandon Cryotome Cryostat (Thermo Fisher Scientific, Ottawa, ON, Canada). They were stained for lipids with Oil red O (Thermo Fisher Scientific, Ottawa, ON, Canada, catalog # AAA1298914) and counterstained for nuclei with Hematoxylin (Sigma- Aldrich, Oakville, ON, Canada, catalog # MHS80-2.5L). The position where each aortic valve leaflet starts to appear was designated as 0 μm for the corresponding valve leaflet and measured in five sections (200 μm apart from the base towards the center of the heart). The coronary artery occlusion was averaged from those five sections. Coronary artery cross sections with atherosclerotic plaques were scored as "atherosclerotic" and those without plaques were scored as "non-atherosclerotic". The quantification was completed in a blinded manner by Dr. George Kluck. Bright-field microscopy with 20x magnification was used to capture all images (Zeiss Axiovert 200M Fluorescence Microscope).

3.10 Anti-Fibrin Staining

The mouse Anti-Human Fibrin monoclonal antibody (mAb) (1:500), designated T2G1 (Accurate Chemical & Scientific Corporation, New York, United States, catalog # NYBT2G1) was used. It reacts only with the Bβ15-42 peptide of the fibrin molecule after thrombin cleavage and the release of both fibrinopeptides (Refer to Figure 5). For staining, transverse cryosections (10 μm) were obtained using Shandon Cryotome Cryostat (Thermo Fisher Scientific, Ottawa, ON, Canada) and stained using the Mouse-On-Mouse (M.O.M) staining kit (Vector Laboratories Canada Inc., Burlington, ON, Canada, catalog #BMK-2202) and an additional blocking reagent, AffiniPure Fab Fragment Goat Anti-Mouse IgG (H+L) (1:11) (Jackson Immunoresearch Laboratory Inc., Pennsylvania, United States, catalog #115-007-003) A Rabbit Anti-Goat IgG (H+L) (1:357) secondary antibody modified with Alexa Fluor 594 dye (1:1000) (Thermo Fisher

Scientific, Ottawa, ON, Canada) was used for immunofluorescent detection. Finally, the slides were counterstained for nuclei with 300 μM DAPI (4′,6-diamidino-2-phenylindole, Invitrogen Canada Inc., Burlington ON, Canada, catalog # D-1306).

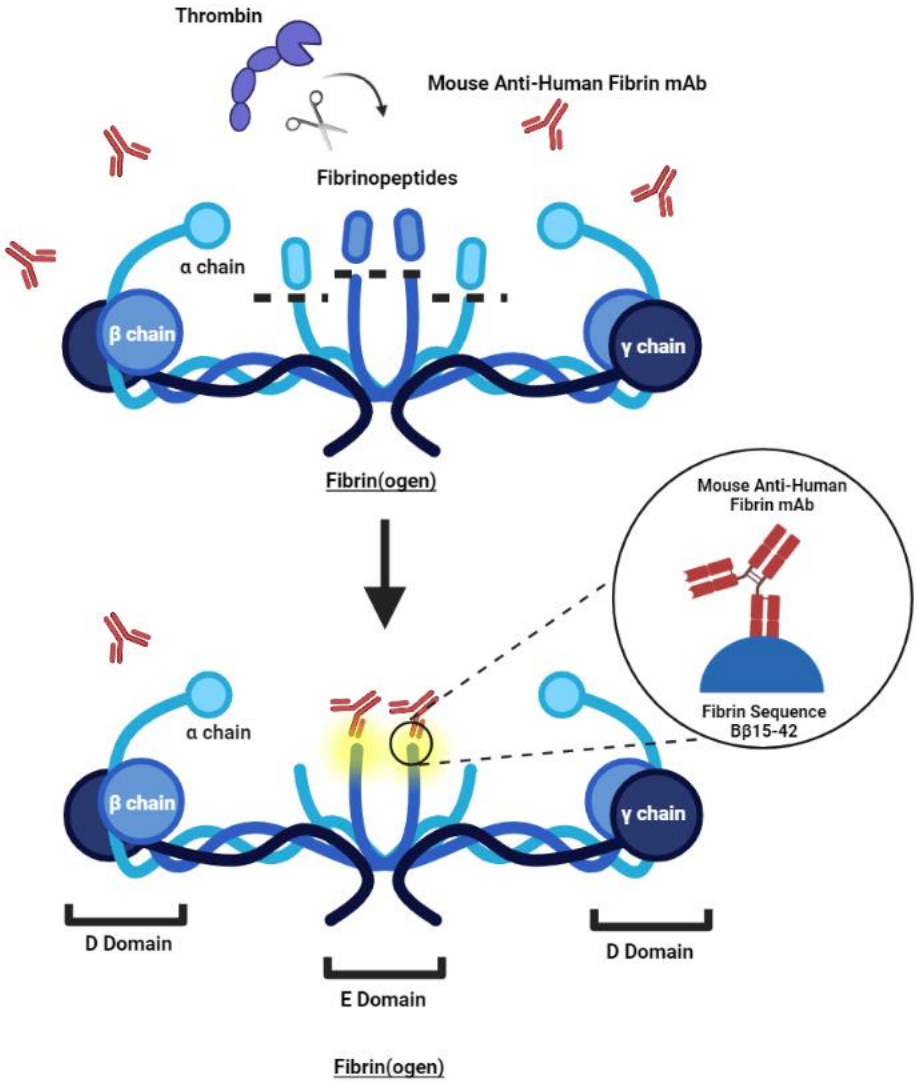

Figure 5: Fibrin Specific mAb-T2G1 This figure illustrates T2G1 mAb specificity towards fibrin and not fibrinogen. It reacts to the Bβ 15-42 sequence on fibrin which is only exposed after thrombin cleavage. *Created in BioRender.com*

3.11 Immunofluorescence Microscopy

Immunofluorescence microscopy was carried out using a Leica DMi8 confocal microscope at 20x magnification. For Alex 594 fluorophore, the maximum excitation and emission wavelengths were 590 nm and 617 nm, respectively, For DAPI, the maximum excitation and emission wavelengths were 358 nm and 461 nm, respectively. Positive staining was defined by greater immunofluorescent intensity compared to negative controls. Immunofluorescence intensity was first established by locating a stained coronary artery and comparing it to a coronary artery that was not stained, and then the stained coronary artery was compared to Secondary Antibody-only control coronary artery. Total Anti-fibrin positive coronary arteries were identified per section and matched with the sections of the Oil Red O-stained adjacent slides to determine the degree of occlusion.

3.12 Myocardial Fibrosis

Transverse cryosections (10 μm) were obtained using Shandon Cryotome Cryostat (Thermo Fisher Scientific, Ottawa, ON, Canada) and stained for fibrosis with Masson's Trichrome (Sigma- Aldrich, Oakville, ON, Canada, catalog # HT15-1KT, HT-10132-1L, HT1079-1SET), which stained healthy myocardium red and collagen fibers blue. The position where each aortic valve leaflet starts to appear was designated as 0 μm for the corresponding valve leaflet and five sections that were 200 μm apart (0 μm, 300 μm, 500 μm, 700 μm, 900 μm) from the base towards the apex of the heart were stained and analyzed. The percentage of fibrosis was calculated by adding the total area of fibrosis and the total area of myocardium in five sections and then dividing those two values to obtain the final percentage. Bright-field

microscopy with 1x magnification was used to capture all images (Zeiss Axiovert 200M Fluorescence Microscope) and Axiovision software was used to quantify the images.

3.13 Statistical Analysis

GraphPad Prism software was used for statistical analysis. For comparison of two groups, data were first subjected to a Shapiro-Wilk test for normality and an F test for equal variance. Those that passed were subjected to a Student's t-test. Those that did not pass the normality test were analyzed by the Mann-Whitney Rank Sum test. For comparison of multiple groups, data were first subjected to the Shapiro-Wilk normality test. Data that passed the normality test were analyzed by One-Way ANOVA. Data that did not pass the normality test were analyzed by the Kruskal-Wallis multiple comparisons test with Dunn's post hoc test. Data are presented as mean ± standard deviation (SD). P values <0.05 were considered statistically significant.

Chapter 4: Results

4.1 Time course of development of aortic sinus and coronary artery atherosclerosis and fibrin deposition in the coronary arteries of SR-B1$^{ko/ko}$ apoE $^{ko/ko}$ mice at 4, 5, and 6 weeks of age

I first analyzed the time course of atherosclerosis development in dKO mice by examining oil-red O/hematoxylin-stained sections of the aortic sinus from mice at 4, 5, and 6 weeks of age. Figure 6A-C shows representative images of oil-red O/hematoxylin-stained sections of aortic sinuses at the level of the intact valve leaflets (aortic root) at 4 (n=7), 5 (n=3), and 6 (n=3) weeks of age, respectively. Figure 6D shows the quantification of the plaque area in the aortic sinus when the first valve leaflet appears (0 μm) to when all three valve leaflets disappear (400 μm). The plaque area was calculated by adding atherosclerotic plaque cross-sectional areas in all three leaflets at the same distance together and the plaque volume was determined by calculating the area under the curve of the plaque area along distance 0 μm to 400 μm. At each given distance, 4-week-old mice had the least amount of plaque development in the aortic sinus while 6-week-old mice had the most. Similarly, the average plaque volume increased from 4 to 6 weeks of age in the dKO mice with average atherosclerotic plaque volumes in 6-week-old mice ($2.88x10^7$ $\mu m^3 \pm 1.6x10^7 \mu m^3$), being significantly greater than those in 4-week-old mice ($1.03x10^6$ $\mu m^3 \pm 6.9x10^5$ μm^3), P=0.0087. (Figure 6E). Figure 7A-C shows representative images of oil-red O/ hematoxylin-stained coronary artery atherosclerosis in dKO mice at 4 (n=6), 5 (n=6), and 6 (n=19) weeks of age, respectively. At 4 weeks of age, there were very few atherosclerotic coronary artery cross sections observed (1.3±0.8), but it increased as the mice aged to 5 (11.3±4.1, P=0.4569) and 6 (31.3±10, P<0.0001) weeks of age (Figure 7G). Furthermore, the number of atherosclerotic coronary artery cross-sections also significantly increased as the mice

aged from 5 to 6 weeks of age, P=0.0397. Similarly, there was very little fibrin deposition in the coronary arteries in the 4-week-old dKO mice, and fibrin deposition in atherosclerotic coronary arteries progressively increased in the 5- and 6-week-old dKO mice (Figures 7D-F). The average number of atherosclerotic coronary artery cross sections with fibrin deposition in the atherosclerotic plaques in dKO mice at 4 (n=8), 5 (n=3), and 6 (n=15) weeks of age were 0.3±0.3, 5±1.9, and 13±4, respectively (4- versus. 5- week-old: P=0.8573, 4- versus. 6- week-old: P<0.0001, 5- versus. 6- week-old: P=0.1845, Figure 7H). Interestingly, fibrin was detected in approximately half of atherosclerotic coronary artery cross sections and the increase in the numbers of fibrin-positive atherosclerotic coronary artery cross-sections mirrored the increase in numbers of atherosclerotic coronary artery cross-sections.

4.2 Treatment of dKO mice with Dabigatran Etexilate (DE)

Having seen very little atherosclerotic plaque development in the aortic sinus and coronary arteries and very little fibrin deposition in atherosclerotic coronary arteries in dKO at 4 weeks of age, and that atherosclerosis in both the aortic sinus and coronary arteries and fibrin deposition in atherosclerotic coronary arteries increased in the dKO mice between 4 and 6 weeks of age, I initiated treatment with DE in mice at 4 weeks of age, for a total of 2 weeks. DE was administered in the diet (6mg/g powdered food) and mice were consumed this medicated diet or a control diet lacking DE, *ad lib*.

A diluted thrombin time assay was performed using platelet-poor plasma collected from the experimental mice fed the DE and control diets and was compared to assays performed with different concentrations of dabigatran to generate a standard curve of diluted thrombin time

versus dabigatran concentration. Dabigatran concentrations ranged from 12.2 to 202.4 ng/ml, and the average was 73±53 ng/ml in plasma from dKO mice fed the diet containing DE (n=16), while dKO mice fed the control diet (n=13) had no detectable dabigatran, as expected (Figure 8). Mice fed the diet containing DE did not exhibit any differences in body weights compared to mice fed the control diet (Figure 9). The average body weights were 18.1±3.3 g and 16.5±2.2 g for males (P=0.2266) and 14.3±1.8 g and 15.2±1.9 g for females (P=0.3187) DE-treated and control mice, respectively (n=6-15). Concentrations of TAT complexes in platelet-poor plasma samples from DE-treated and control dKO mice were determined by ELISA (Figure 10). The average TAT complex concentration in plasma from control dKO mice was 17.8±8.5 ng/ml (n=11). There was a significant decrease in the average plasma level of TAT complexes in DE-treated mice (4.1±5.1 ng/ml, n=16), P< 0.0001. This suggests the competitive binding of DE on the active site of thrombin occupying antithrombin's binding site resulting in a reduction of the TAT complexes formed. To further evaluate the effects of DE feeding on thrombin activation, thrombin generation assays were performed to determine circulating prothrombin potential upon stimulation in plasma samples from the control and DE-fed dKO mice. The thrombograph in Figure 11A demonstrates the average thrombin levels per minute for the entire duration of the assay (91 minutes). It showed an overall reduced capacity for circulating prothrombin to become stimulated in the plasma prepared from the DE-treated mice (green line) compared to the control mice (black line). Particularly, there was a significant increase in the lag time (91±0 minutes) in DE-treated mice (n=16), p<0.0001, as well as a significant reduction in peak thrombin levels (8.2±7.7 nM), p=0.0012, and endogenous thrombin potential (338.1±106.3 nM*mins), p<0.0001, compared to the control mice (n=12, 7±1.28 minutes; 41.89±31.2 nM; 1204.27±932.9 nM*mins) (Figures 11B-D).

4.3 DE treatment significantly reduced aortic sinus and coronary artery atherosclerosis in dKO mice

DE treatment has previously been reported to reduce atherosclerosis development in the aortic sinus of SKO mice[32,33,46,47]. Therefore, I first analyzed atherosclerotic plaque sizes in oil-red O/ hematoxylin-stained sections of the aortic sinuses of DE-treated and control dKO mice (Figures 12A-B). DE-treated dKO mice (n=8, green line) exhibited apparent reductions compared to control mice (n=9, black line) in plaque cross-sectional areas of atherosclerotic plaques along the entire 400 μm stretch of the aortic sinus analyzed (Figure 12C). Atherosclerotic plaque volumes calculated as the area under the curve of plaque area versus distance were significantly lower in DE-treated mice (n=8, $1.1x10^7 \pm 6.7x10^6$ μm^3) compared to control mice (n=14, $2.2x10^7 \pm 1.04x10^7$ μm^3; Figure 12D), P=0.0103.

Figure 13A shows a representative image of an Oil red O/hematoxylin-stained coronary artery cross-section that is free of atherosclerotic plaque and Figures 13B-D show a series of coronary arteries that are filled with atherosclerotic plaques. Analysis of counting all atherosclerotic coronary artery cross sections starting from the base of the heart to when the first aortic sinus leaflet appears (a total of five sections that were 200 μm apart) revealed that there was a significant reduction in the numbers of coronary artery cross sections containing atherosclerotic plaques in the DE treated compared to control dKO mice (Figure 13E). DE-treated mice (n=9) exhibited an average of 10±6 atherosclerotic coronary artery cross-sections whereas control dKO mice (n=19) exhibited 27±12 atherosclerotic coronary artery cross-sections ($P<0.0001$).

To examine the effects of DE treatment on fibrin deposition in atherosclerotic coronary arteries in dKO mice, adjacent cross-sections of hearts were stained with either oil red O/hematoxylin and subjected to bright-field microscopy (Figures 14A and C) to identify lipid-rich atherosclerotic plaques in coronary artery cross sections, or the T2G1 mAb specific for the Bβ15-42 peptide exposed in fibrin after thrombin cleavage of fibrinogen, and subjected to confocal fluorescence microscopy (Figures 14B and D). Quantification of the numbers of atherosclerotic coronary artery cross sections that were positive for the anti-fibrin antibody staining across five sections (200 μm apart) starting from the base of the heart until the appearance of the first aortic sinus valve leaflet, demonstrated that DE treatment of dKO mice (n=8) significantly reduced the number of atherosclerotic coronary artery cross sections with fibrin deposition (6±4) compared to control dKO mice (n=11, 14±5), P=0.0059.

4.4 Effects of DE treatment on inflammatory cytokines and, markers of myocardial damage in dKO mice

Plasma levels of IL-6 were substantially, and MCP-1 was moderately elevated, whereas levels of TNF-α were unchanged in 6-week-old dKO mice compared to SKO mice (Figures 15A-C). DE treatment of the dKO mice resulted in a significant reduction in plasma IL-6 levels (Figure 15A; means ± standard deviations: 440±260 versus 2260±2300 pg/ml, respectively. P=0.0157) but did not affect plasma levels of either MCP-1 or TNF-α (Figure 15B and C). Plasma levels of high sensitivity cTnI were measured as a marker of cardiomyocyte damage (Figure 16A). Plasma levels of high sensitivity cTnI were substantially elevated (n= 11, 48.6±33.7 ng/ml) compared to similarly aged SKO mice (n= 6, 8.8±0.3 ng/ml), P=0.0027. DE treatment of the dKO mice was accompanied by a substantial reduction in plasma cTnI levels

(n=11, 12.6±7.8 ng/ml; P=0.0001) compared to control dKO mice. Examination of heart weights normalized to tibia lengths (Figure 16B) showed that control dKO mice (n=26) exhibited significantly increased heart weight to tibia length ratio (0.08±0.01) compared to similarly aged SKO mice (n=47, 0.06±0.01; P<0.0001). DE treatment of the dKO mice did not affect heart weight to tibia length values measured (n= 24, 0.08±0.02; P >0.9999). Figure 16C-D shows representative images of trichrome-stained cross-sections of hearts from control and DE-treated dKO mice, respectively. Healthy myocardium appears red, and collagen-rich areas appear blue. Analysis of the extent of blue staining across a series of five heart sections that were 200 μm apart from the base of the heart to the appearance of the first aortic sinus valve leaflet in each mouse revealed no significant differences in the amount of collagen deposition in the myocardium between DE treated (n=8) and control (n=6) dKO mice (13.8±8.3% versus 19.2±14.8% of myocardial area positive for collagen, P=0.8518; Figure 16E).

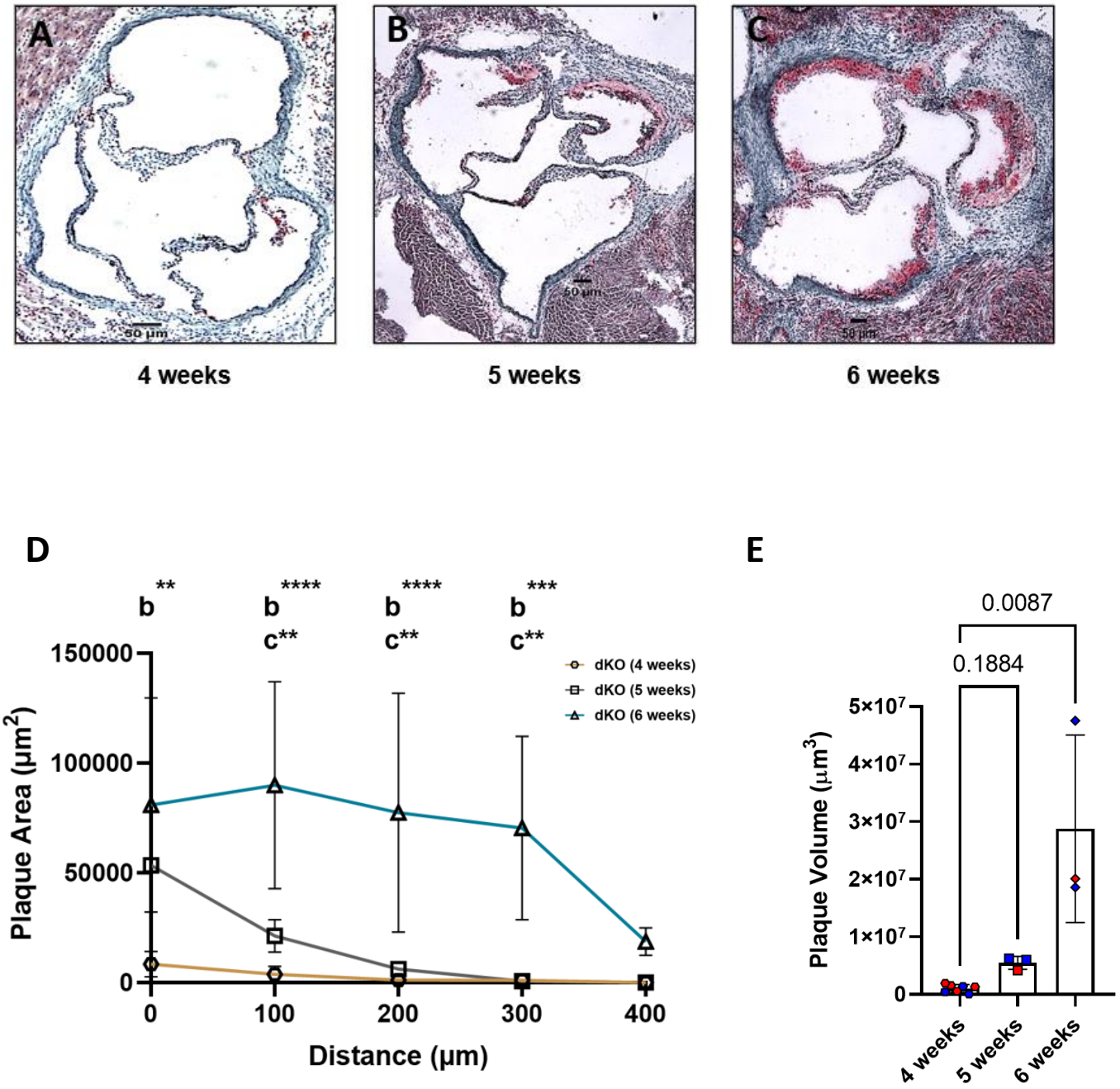

Figure 6: Time Course Development of Atherosclerosis in the Aortic Sinus of dKO mice Representative images of aortic sinus atherosclerosis between dKO mice at 4 (Figure A), 5 (Figure B), and 6 (Figure C) weeks of age on normal pallet diet. Figure D shows quantification of the plaque area in the aortic sinus from distances 0µm to 400µm between dKO mice at 4 (brown line), 5 (grey line), and 6 (blue line) weeks of age. Two-way ANOVA test (a: 4- versus 5-week-old, b: 4- versus 6-week-old, c: 5- versus 6-week-old), **P < 0.01, ***P < 0.001, ****P < 0.0001. Figure E shows the average plaque volume in the aortic sinus between dKO mice at 4,5, and 6 weeks of age was $1.03x10^6$ μm^3, $5.48x10^6$ μm^3, and $2.88x10^7$ μm^3, respectively. Blue points represent Males; Red points represent Females. Kruskal-Wallis test

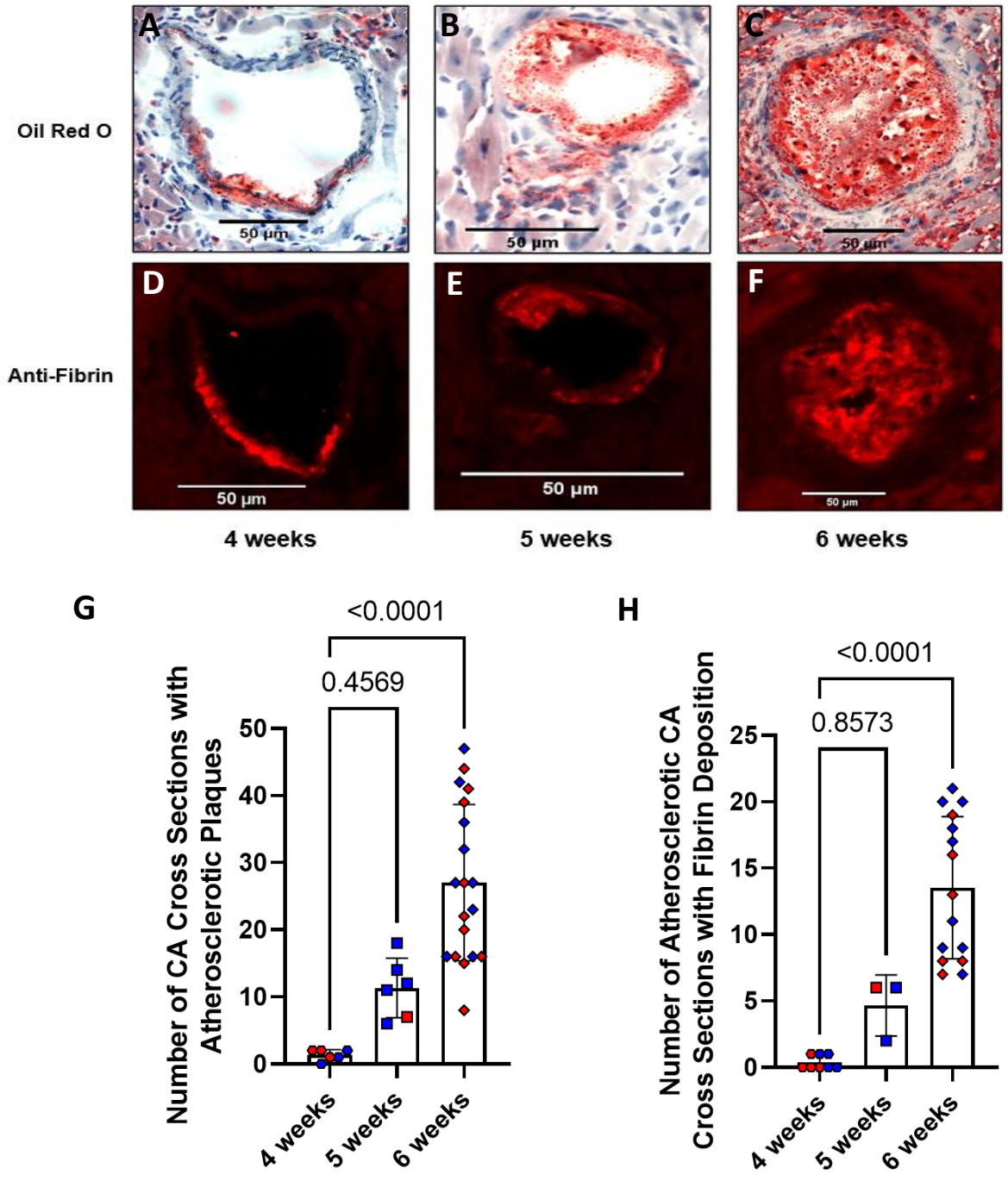

Figure 7: Time Course Development of Atherosclerosis and Fibrin Deposition in the Coronary Arteries of dKO mice Representative images of coronary artery atherosclerosis and fibrin deposition between dKO mice at 4 (Figure A&D), 5 (Figure B&E), and 6 (Figure C&F) weeks of age. Each age group represents the same coronary artery stained for both lipids and anti-fibrin. The average number of coronary artery cross sections with atherosclerotic plaques between dKO mice at 4, 5, and 6 weeks of age was 1, 11, and 31, respectively, and was only significantly different between the 4- and 6- week-old dKO mice, $P<0.0001$. (Figure G). The average number of atherosclerotic coronary artery cross sections with fibrin deposition between dKO mice at 4,5, and 6 weeks of age was 0, 5, and 13, respectively, and was only significantly different between the 4- and 6- week-old dKO mice, $P<0.0001$. (Figure H). Blue points represent Males; Red points represent Females. Kruskal-Wallis test.

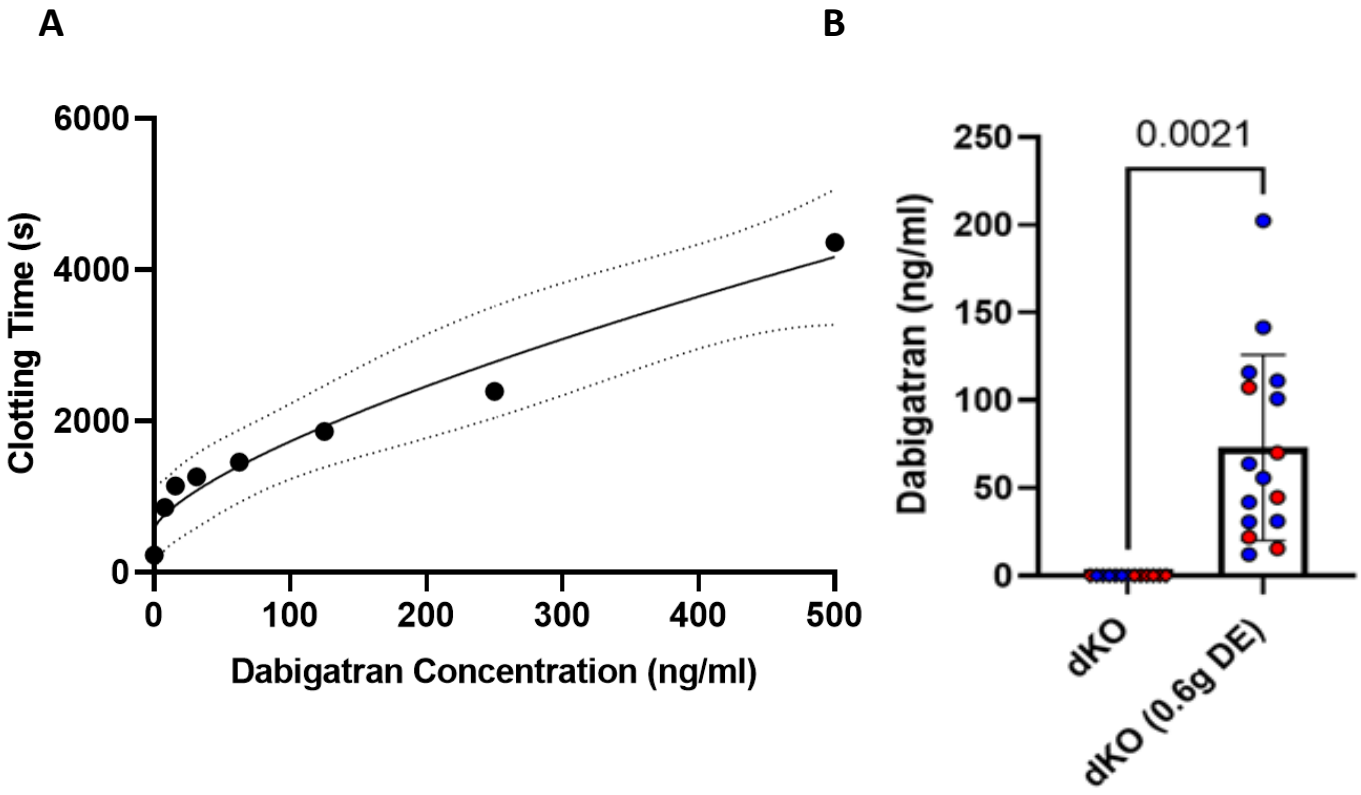

Figure 8: Plasma Dabigatran Concentration The standard curve was created by measuring varying (0-500 ng/ml) Dabigatran concentration and its corresponding clotting time. The R-squared value of the curve was 0.96. (Figure A). In DE-treated mice, Dabigatran concentration ranged from 12.2- 202.4 ng/ml, and the average was 73.0 ng/ml, while there were no detectable amounts of Dabigatran in the control dKO mice, P=0.0021. (Figure B). Blue dots represent males and red dots represent females. Mann-Whitney test.

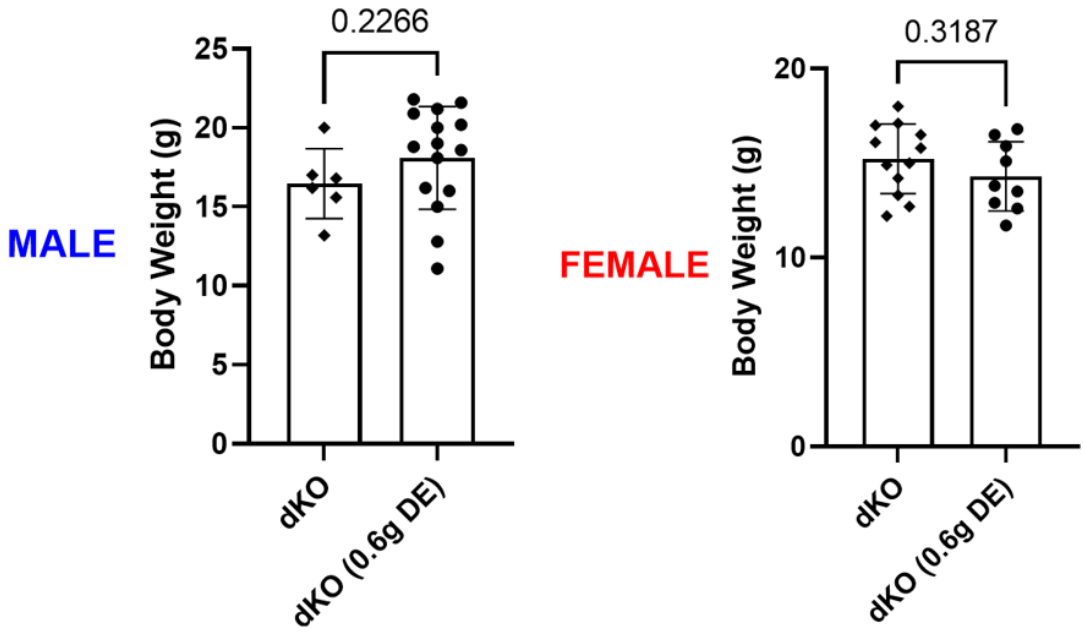

Figure 9: Body Weight of DE treated and Control dKO mice between Males and Females The average male body weight of DE treated dKO mice was 18.1g and the control dKO mice was 16.5g, P=0.2266. The average female body weight of DE-treated dKO mice was 14.3g and the control dKO mice was 15.2g, P=0.3187. Mann-Whitney test.

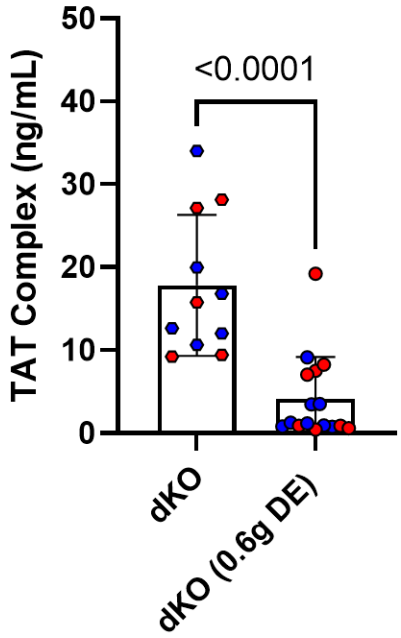

Figure 10: Thrombin- Antithrombin (TAT) Complex The average concentration of TAT complexes in DE-treated dKO mice was 4.1 ng/ml and 17.8 ng/ml in the control dKO mice, P <0.0001. Blue dots represent males and red dots represent females. Mann-Whitney test.

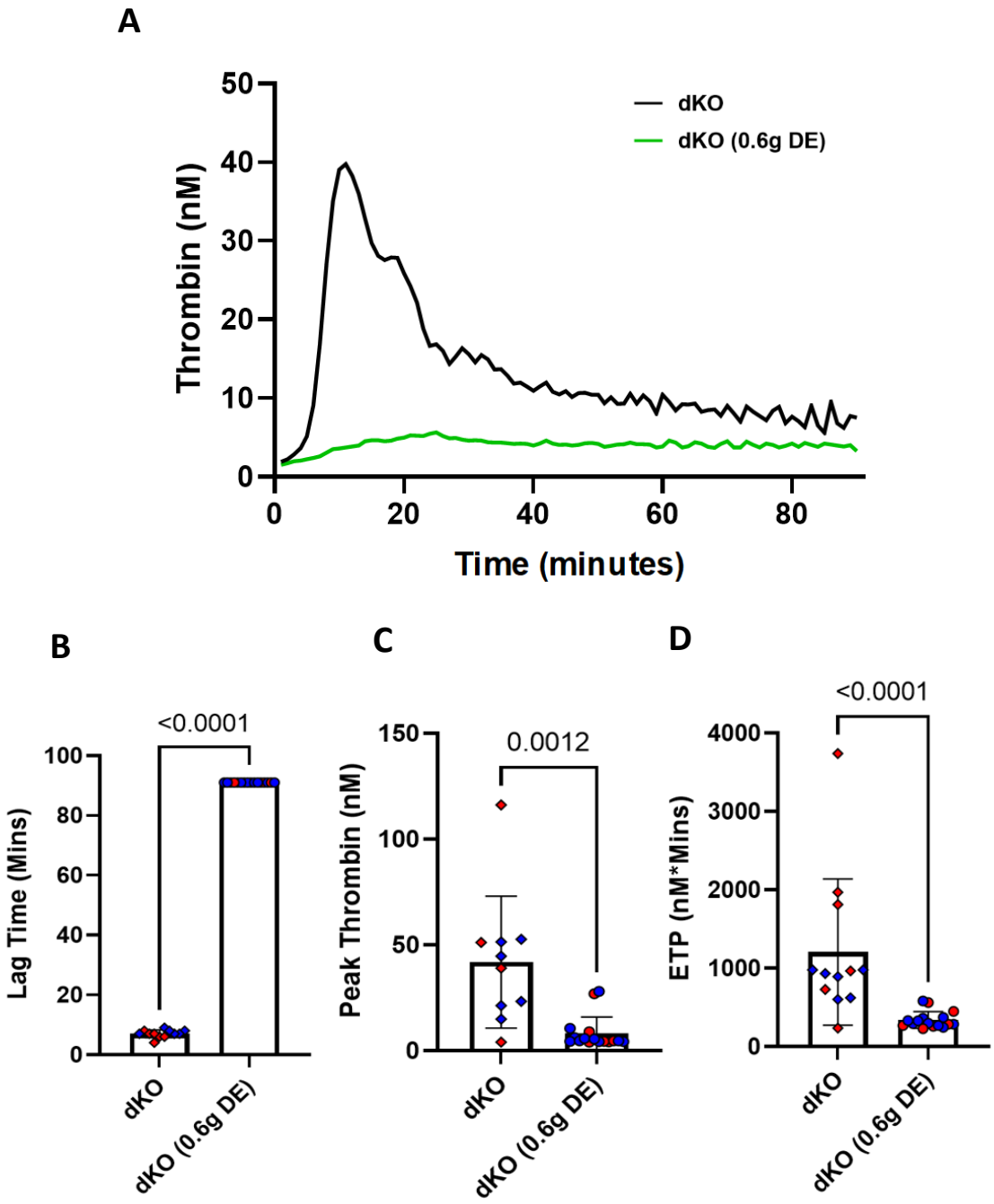

Figure 11: Thrombin Generation Assay Figure A shows a thrombograph displaying the average endogenous thrombin activity for 91 minutes between DE-treated dKO mice (n=17 green line) and control dKO mice (n=16, black line). The average time it took for endogenous thrombin to reach peak levels in DE-treated dKO mice was 91 minutes and 7 minutes for control dKO mice, P<0.0001 (Figure B). The average peak thrombin levels in DE-treated dKO mice were 8.2 nM and 41.9 nM for control dKO mice, P=0.0012 (Figure C). The Endogenous Thrombin Potential (ETP) in DE-treated dKO mice was 338.1 nM*mins and 1204.3 nM*mins for control dKO mice, P<0.0001 (Figure D). Blue dots represent males and red dots represent females. Mann-Whitney test.

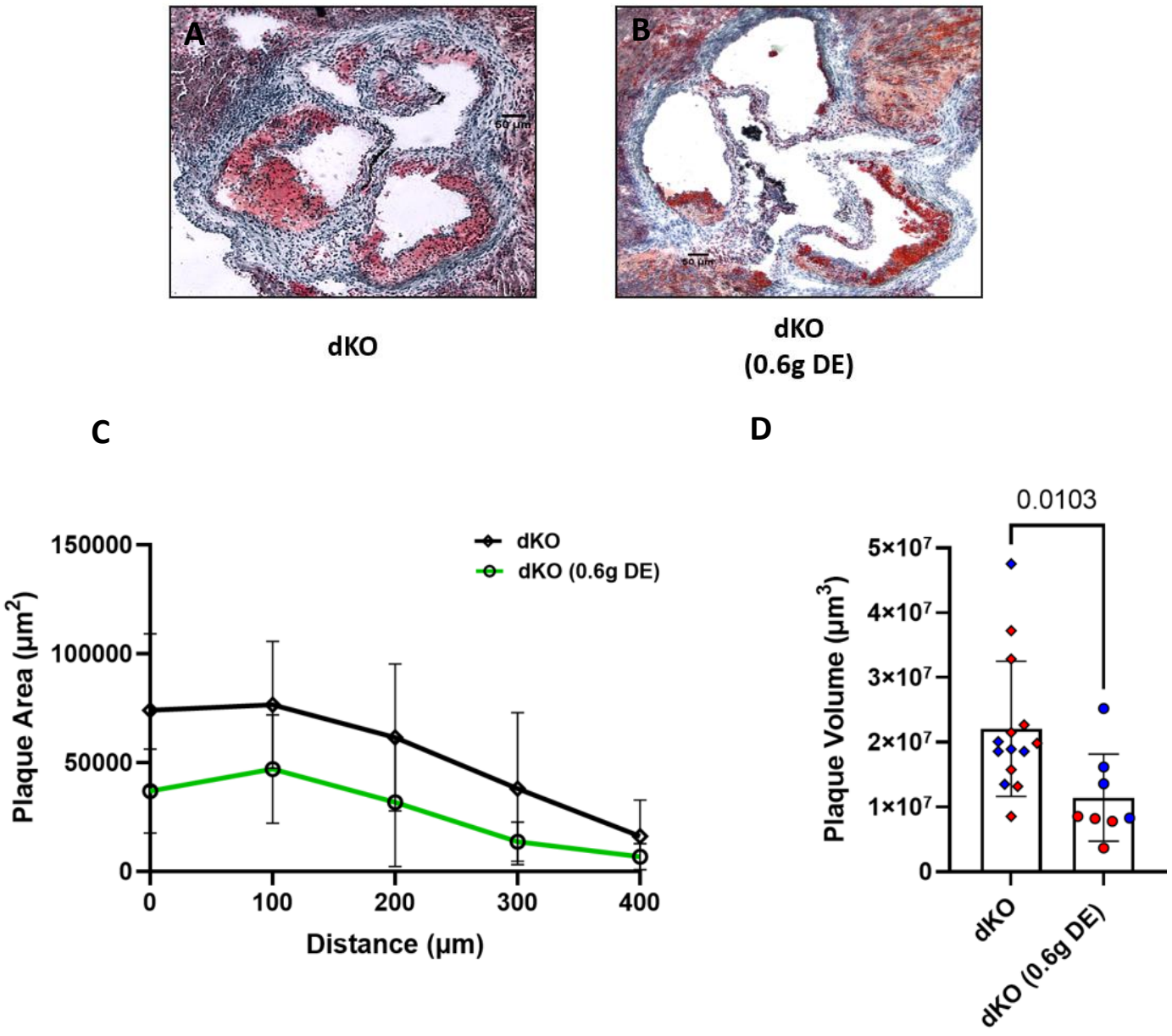

Figure 12: Aortic Sinus Atherosclerosis Representative images of the aortic sinus of DE-treated dKO mice (Figure B) and control dKO mice (Figure A). Figure C shows the average plaque area in the aortic sinus at distances 0µm to 400µm between DE-treated dKO mice (green line) and control dKO mice (black line). The average plaque volume in the aortic sinus for DE-treated dKO mice was $1.1x10^7$ μm^3 and $2.2x10^7$ μm^3 for the control dKO mice, P=0.0103 (Figure D). Blue dots represent males and red dots represent females. Two-way ANOVA test. Mann-Whitney test.

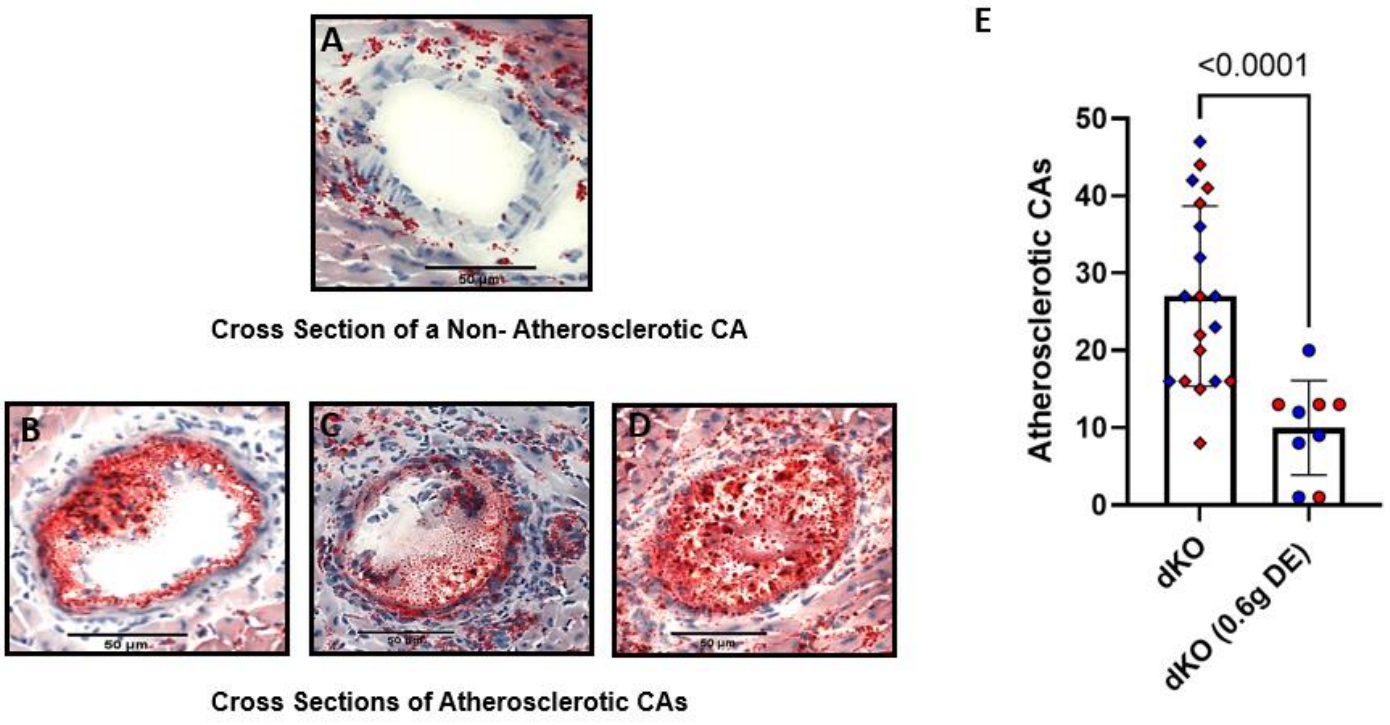

Figure 13: Coronary Artery Atherosclerosis Representative images of Oil Red O-stained coronary artery cross sections that did not have atherosclerotic plaques, termed Non-Atherosclerotic CAs (Figure A), and coronary artery cross sections that have atherosclerotic plaques, termed atherosclerotic CAs (Figures B-D). The average number of CAs with atherosclerotic plaques in DE-treated dKO mice was 10 and 27 for the control dKO mice, $p<0.0001$ (Figure E). Blue dots represent males and red dots represent females. Mann-Whitney test.

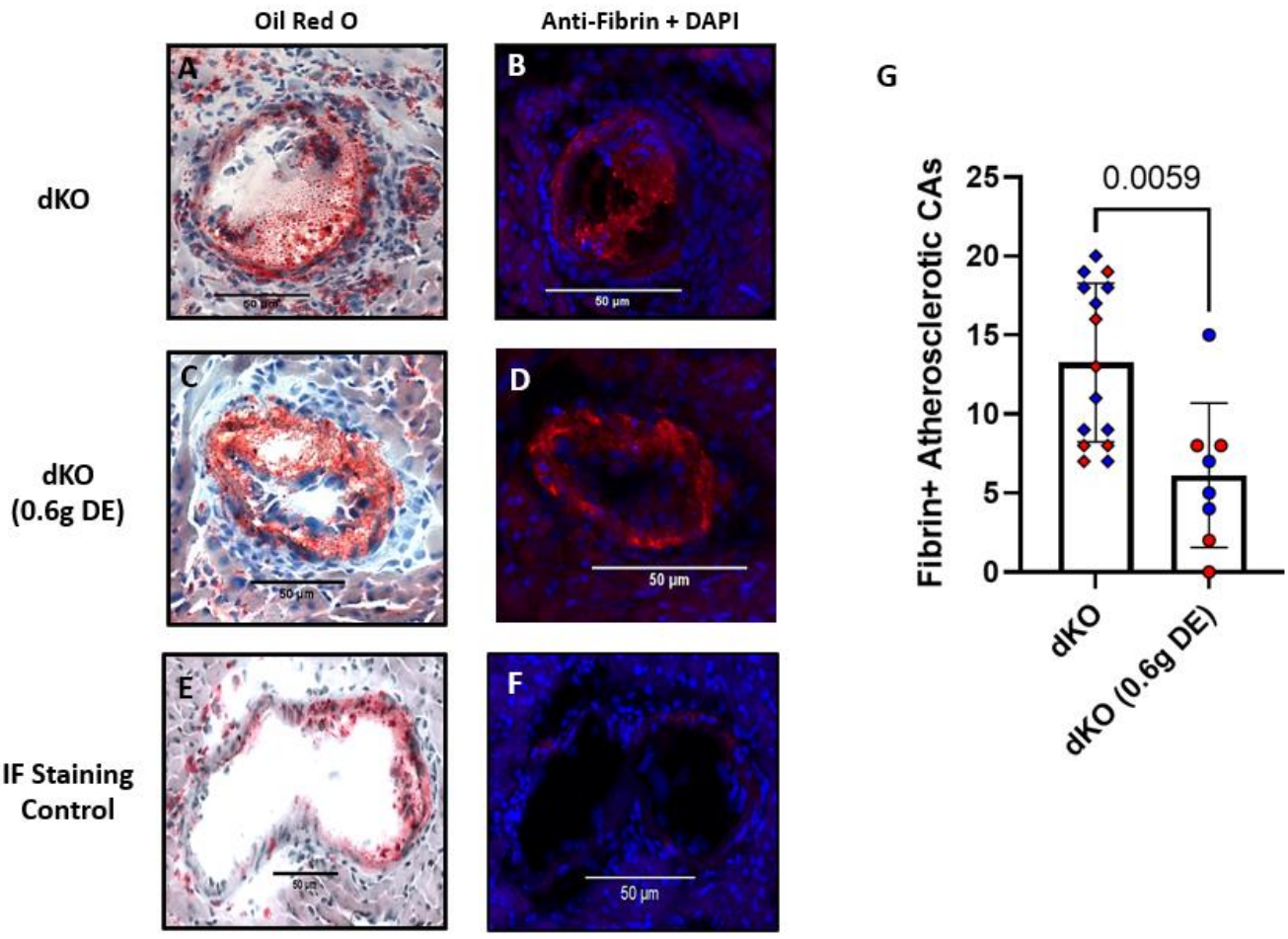

Figure 14: Anti-Fibrin Staining in Atherosclerotic Coronary Arteries Figures A-F show representative images of the same cross-section CA stained with Oil Red O, Anti-fibrin, and DAPI. Red fluorescence indicates fibrin deposition. Figures A and B are CA cross-sections from control dKO mice. Figures C and D are CA cross-sections from DE-treated dKO mice. Figure F is an immunofluorescent staining control CA cross-section that was stained without Primary antibody and Figure E is the corresponding CA cross-section stained with Oil Red O. The average number atherosclerotic CA cross-sections with fibrin deposition in dKO mice receiving DE treatment was 8 and 11 for control dKO mice, p=0.0059 (Figure G). Blue dots represent males and red dots represent females. Mann-Whitney test.

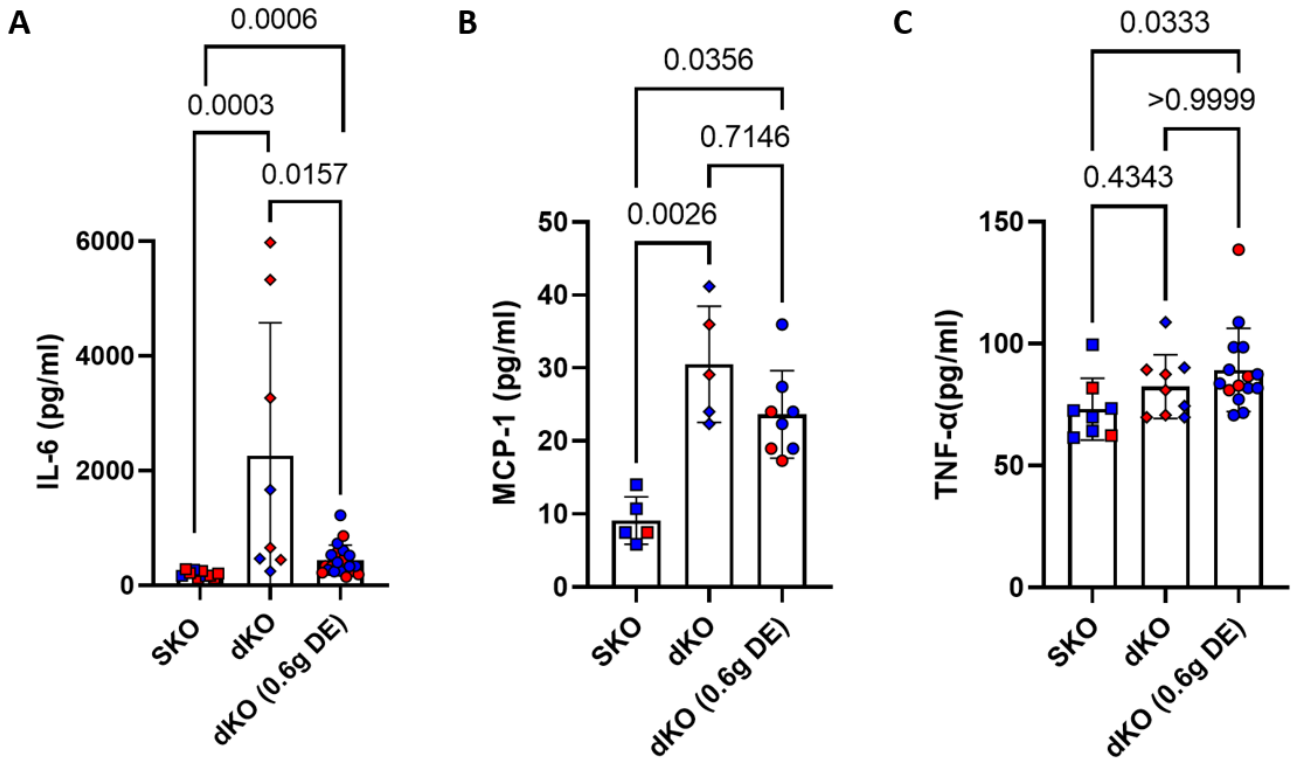

Figure 15: Inflammatory Cytokines The average concentration of IL-6 in SKO mice (196.8 pg/ml) was significantly lower compared to both control dKO mice (2257.5 pg/ml), P=0.0003, and DE-treated dKO mice (439.9 pg/ml), P=0.0006. The average concentration of IL-6 was also significantly lower in DE-treated dKO mice compared to control dKO mice, P=0.0157 (Figure A). The average concentration of MCP-1 was significantly lower in SKO mice (9.1 pg/ml) compared to both control dKO mice (30.5 pg/ml), P=0.0026, and DE-treated dKO mice (23.6 pg/ml), P=0.0356. However, no significant differences were found between DE-treated dKO mice and control dKO mice, P=0.7146 (Figure B). The average concentration of TNF-α was significantly lower in the SKO mice (73.1 pg/ml) compared to the DE-treated dKO mice (89.2 pg/ml), P=0.0333. However, no significant differences were found between SKO mice and control dKO mice (82.4 pg/ml), P=0.4343, as well as, between DE-treated dKO mice and control dKO mice, P>0.9999 (Figure C). Blue points represent Males; Red points represent Females. Mann- Whitney test. Kruskal-Wallis test.

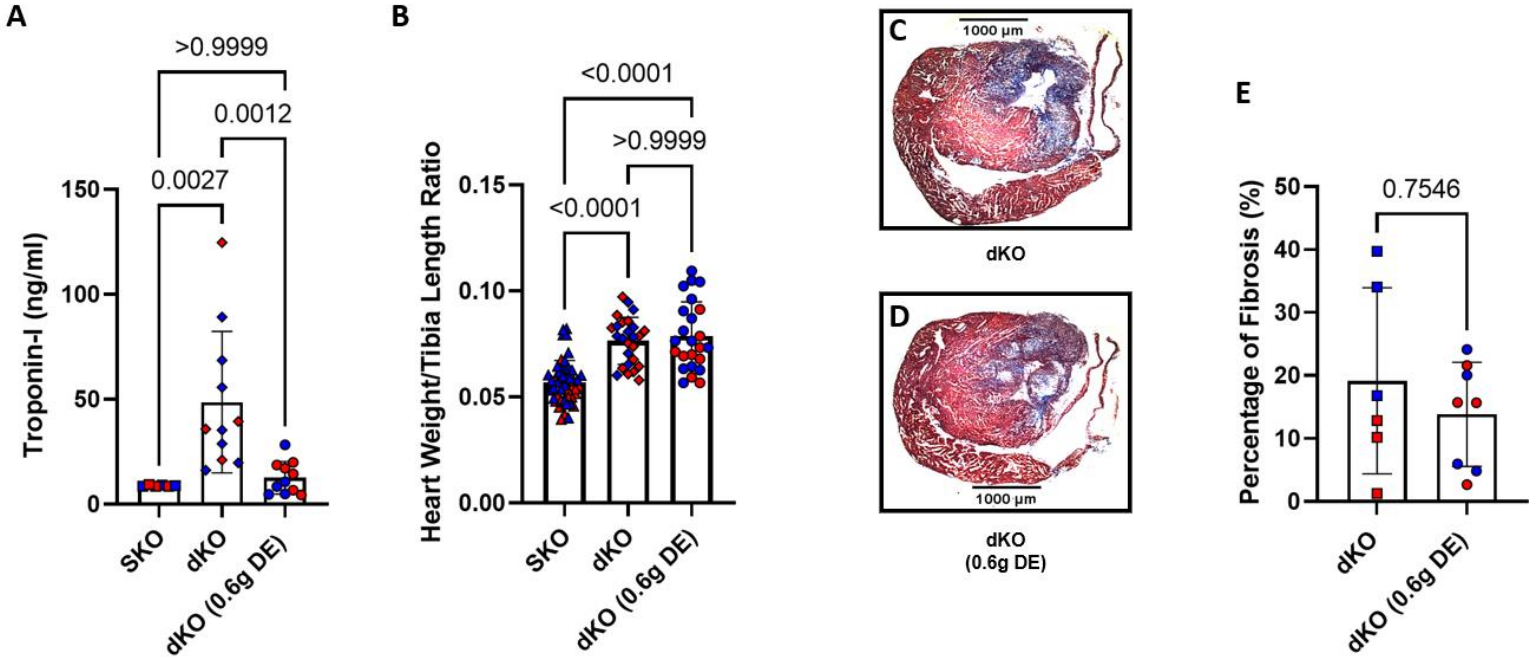

Figure 16: Myocardial Fibrosis The average concentration of troponin-I was significantly lower in SKO mice (8.8 ng/ml) compared to control dKO mice (48.6 ng/ml), P=0.0027, but not compared to DE-treated dKO mice (12.6 ng/ml), P>0.9999. However, DE treatment significantly lowered troponin-I levels compared to the dKO control mice, P=0.0012 (Figure A). The average heart weight to tibia length ratio was significantly lower for SKO mice (0.06) compared to both control dKO mice (0.08) and DE-treated dKO mice (0.08), p<0.0001. However, there were no significant differences in the heart weight to tibia length ratio between control dKO and DE-treated dKO mice, p>0.9999 (Figure B). Figures C and D show representative images of Trichrome stained myocardium of control dKO mice and DE-treated dKO mice at the same distance, respectively. There were no significant differences in the average percentage of fibrosis levels between control dKO mice (19.2%) and DE-treated dKO mice (13.8%), p=0.7546 (Figure E). Blue dots represent males and red dots represent females. Kruskal-Wallis test. Mann-Whitney test.

Chapter 5: Discussion

Previous study has demonstrated that the dKO mice were hypercholesteremic, develop extensive cardiac deficits, and experience multiple myocardial infarctions leading to premature deaths[44]. Furthermore, fibrin was reported to be detected in a cross-section of a coronary artery in a dKO mouse, however, neither the time course nor the extent of fibrin deposition in atherosclerotic coronary arteries of these mice was characterized. Therefore, the first objective of the study was to establish the onset of coronary artery disease development in the dKO mice. The results showed that dKO mice fed with a standard laboratory diet at 4 weeks of age had minimal coronary artery and aortic sinus atherosclerosis. However, both coronary artery and aortic sinus atherosclerosis developed rapidly over the next two weeks such that substantial atherosclerosis was present in both the aortic sinus and coronary arteries in mice by 6 weeks of age. By 6 weeks of age, these mice also exhibited systemic inflammation as evidenced by elevated circulating IL-6 and MCP-1 levels and had extensive cardiac fibrosis and cardiomyocyte damage. Furthermore, there was also greater fibrin detection in the coronary arteries of these mice. Taken together, this indicates that dKO mice at 4 weeks of age were in the early stage of atherosclerosis development in which the disease had just begun to develop but by 6 weeks of age, the disease was severely developed with systemic inflammation, coagulation activation, and plasma markers of cardiac damage.

The next objective was to better understand the involvement of the coagulation pathway in atherosclerosis development by testing the effects of altering fibrin deposition in the coronary arteries. This was achieved by targeting the serine protease, thrombin, with a direct thrombin inhibitor DE. Thrombin was chosen as the target because it is a functionally diverse protein involved in both inflammation and coagulation, which are all processes important to the

development of atherosclerosis[23]. It plays a crucial role in the coagulation pathway because it is not only required for the conversion of fibrinogen to fibrin but is also necessary for the stabilization of a fibrin clot since it is capable of amplifying its production by activating many other clotting factors along the intrinsic pathway. On the other hand, the proinflammatory effects of thrombin are mediated by PAR -1 signalling[23,48]. When activated, the extracellular N-terminus is cleaved predominately by thrombin but not exclusively, other serine proteases such as FXa, plasmin, Kallikriens, APC, and MMP-1 are also capable of such cleavage, exposing a new N-terminus that act as a tethered ligand by binding intramolecularly to the receptor to trigger transmembrane signalling[48].

To study the effects of direct thrombin inhibition in spontaneous coronary artery atherosclerosis development, dKO mice were treated with DE at 4 weeks of age for a period of two weeks. The treatment of DE significantly reduced the capacity of thrombin generation and TAT complex formation, as well as plaque development in the aortic sinus and coronary arteries at 6 weeks of age. There was significantly less plaque detected in the aortic sinus of DE-treated mice, and the number of coronary artery cross-sections with atherosclerotic plaques were significantly less in dKO mice that received DE treatment compared to the control. Furthermore, DE treatment led to an overall reduction in the number of atherosclerotic coronary artery cross-sections that were positive for fibrin. These findings were consistent with previous literature on the beneficial effects of DE treatment and atherosclerotic plaque development in the aortic sinus[32–34,47]. However, the current study was the first to show that DE treatment reduced atherosclerosis and fibrin deposition in the coronary arteries.

Based on previous studies, one can speculate that this beneficial effect of reduced plaque development may have been a result of DE's ability to improve endothelial function and reduce

monocyte/macrophage infiltration, which in turn decreases LDL entry opportunity and foam cell formation[33,46,49]. Another novel finding from this study was the reduced fibrin deposition found in atherosclerotic coronary artery cross-sections. This was an expected finding because dabigatran is capable of binding to both free- and clot-bound thrombin reducing thrombin's catalytic capacity at converting fibrinogen to fibrin. However, in the current study, the inhibition of thrombin's catalytic site only reduced but did not prevent fibrin deposition in the coronary arteries. This could have been a result relating to the dosage of DE given to these mice, more specifically, the dosage was simply too low to fully inhibit thrombin thus allowing thrombin to continue its catalytic activity of cleaving fibrinogen and leading to fibrin deposition. Alternatively, the observation of fibrin deposition in the coronary arteries despite thrombin inhibition may suggest another mechanism regulating the interaction between thrombin and fibrin(ogen) other than through the thrombin's catalytic site. Previous studies have shown that the conversion of fibrinogen to fibrin relies on both the catalytic site and exosite I on thrombin and that both thrombin's exosite I and II are capable of interacting with fibrin at different binding affinities [50,51]. Therefore, while dabigatran inhibits the catalytic site of thrombin, fibrinogen may still be capable of interacting with thrombin via thrombin's exosites I and II leading to fibrin deposition. However, this possibility remains to be explored.

The pro-inflammatory effects of thrombin were assessed by measuring levels of IL-6, MCP-1, and TNF-α. Prior to DE treatment, IL-6 and MCP-1 levels were increased in dKO mice compared to SKO mice, while no changes were found in TNF-α levels. After DE treatment, there was a reduction in IL-6 levels and a trend towards a reduction in MCP-1 levels in DE-treated mice compared to control dKO mice. Although significance was not reached in MCP-1 levels, previous studies have shown that direct thrombin inhibition reduced MCP-1 levels in plasma and

was accompanied by reduced monocyte/macrophage infiltration at the site of plaque lesion[46,52]. In contrast, no significant differences were found in TNF-α levels between DE-treated and control dKO mice. These findings suggest that direct thrombin inhibition reduces selective proinflammatory cytokine production and that this is most likely a result of inhibiting thrombin-mediated PAR-1 signaling pathways.

The body weight and heart-to-tibia length ratio of DE-treated mice did not differ significantly from control dKO mice. Furthermore, DE treatment did not reduce the extent of fibrosis present in the hearts of these mice, even though there was a significant reduction of troponin-I levels suggesting less cardiomyocyte damage. This discrepancy between cardiac fibrosis and cardiomegaly with reduced cardiomyocyte damage can potentially be explained by the role of thrombin mediated PAR-1 signaling. A recent study by Dolleman and colleagues (2022) found that while thrombin's active site is fully inhibited by dabigatran, PAR-1 may still interact via thrombin's exosite I and potentially enhanced the expression of the receptor on endothelial surface[53]. A similar finding by Achilles and colleagues (2017) demonstrated that there was an increase in platelet reactivity in patients receiving dabigatran treatment due to enhanced expression of PAR-1 density on platelets[54]. Therefore, the ability of thrombin to continue to activate PAR-1 signaling even in the presence of dabigatran was demonstrated in endothelial cells and platelets. Thrombin can activate PAR-1 signaling in cardiac fibroblasts to increase their proliferation, migration, and differentiation into collagen-producing cells, contributing to cardiac fibrosis[55]. However, whether this depends on thrombin binding to PAR-1 via thrombin's exosite I and thus may still occur in the presence of dabigatran remains to be explored.

In the current study decreased levels of troponin-I were also detected which suggests reduced cardiomyocyte damage. This can potentially be explained by distinct PAR-1 signaling pathways found between cardiac fibroblasts and cardiomyocytes[56]. Sabri and colleagues (2002) showed that in cardiac fibroblasts, thrombin mediated PAR-1 activation led to strong extracellular signal-regulated kinase (ERK) and Akt signalling with prominent epidermal growth factor receptor (EGFR) transactivation, whereas in cardiomyocyte, thrombin mediated PAR-1 activation led to ERK, and modestly Akt signalling that required little to no EGFR transactivation [56], suggesting that there are multiple signalling pathways regulating the effects of PAR-1 in different cell types, and whether there are also differential effects of thrombin binding versus thrombin-mediated proteolytic activation on signaling by PAR-1 or other PARs in different cell types remains to be explored. However, if there are differences then dabigatran may exert different effects on thrombin-mediated PAR activation in different cell types.

In summary, this study established the time course development of atherosclerosis in dKO mice, and importantly, the time course and extent of fibrin deposition in atherosclerotic coronary arteries. At 4 weeks of age, there were no signs of aortic sinus and coronary artery atherosclerosis. In addition, no signs of cardiac fibrosis and very minimal activation of the inflammatory and coagulation pathways. However, by 6 weeks of age, these mice develop extensive aortic sinus and coronary artery atherosclerosis and experience widespread cardiac fibrosis and inflammation. Furthermore, there was greater fibrin deposition detected in the coronary arteries of these mice. The study also explored the effects of direct thrombin inhibition in atherosclerosis development. Overall, in a spontaneous coronary artery disease mouse model the direct inhibition of thrombin reduced systemic inflammation, atherosclerotic plaque development in the aortic sinus and coronary arteries, and fibrin deposition in the atherosclerotic

coronary arteries. It also reduced cardiomyocyte damage, but no changes were seen in cardiac fibrosis.

Conclusion

Taken together, the current study was the first to demonstrate the time course and extent of fibrin deposition in the coronary arteries of SR-B1$^{ko/ko}$ apoE$^{ko/ko}$ mice. It was also the first study to show the effects of direct thrombin inhibition by DE in a spontaneous coronary artery atherosclerosis murine model. The study found that DE treatment reduced aortic sinus and coronary artery atherosclerosis, as well as reduced fibrin deposition in the coronary arteries. It also showed that DE treatment reduced inflammatory cytokines selectively. While improvements were seen in atherosclerosis development and fibrin deposition, direct thrombin inhibition did not improve cardiac fibrosis experienced in these mice. This suggests an alternative mechanism regulating the proinflammatory responses exerted by thrombin, and one such mechanism relates to the role of thrombin mediated PAR-1 signalling. In atherosclerosis, the improvement seen by DE treatment seemed to be masked by the unfavourable interaction between thrombin's exosite I and PAR-1. While previous study has demonstrated in endothelial cells that when the active site of thrombin is catalytically inhibited by dabigatran, the exosites remain functional, which provides an opportunity for thrombin to continue to elicit proinflammatory signaling via PAR-1, though this remains to be tested experimentally in other cell types such as cardiac fibroblasts. Furthermore, previous study has shown distinctive thrombin mediated PAR-1 signalling pathways between cardiac fibroblasts and cardiomyocytes which may be a potential explanation for the opposite results seen in cardiac fibrosis and cardiomyocyte damage in the current study.

In conclusion, this thesis demonstrated that the SR-B1$^{ko/ko}$ apoE$^{ko/ko}$ spontaneous coronary artery atherosclerosis mouse model has the potential in being utilized to study human coronary

artery disease as it not only exhibited many cardinal features of human coronary artery disease but also responded similarly to clinical treatment (i.e., Dabigatran). While direct thrombin inhibition yielded beneficial effects on reducing plaque development, it also yielded some unexpected effects on cardiac remodeling. Previous studies have alluded to the potential role of thrombin mediated PAR-1 signalling as the alternative mechanism regulating thrombin's effect. Therefore, it may be worthwhile for future studies to explore the effects of direct inhibition or complete deletion of thrombin versus PAR-1 on coronary artery atherosclerosis to better understand the mechanistic role of thrombin and whether direct PAR-1 inhibition is a better approach in treating inflammatory diseases such as atherosclerosis.

References

1. Statistics Canada. Leading causes of death, total population, by age group. https://doi.org/10.25318/1310039401-eng.

2. Public Health Agency of Canada. Heart disease in Canada: Highlights from the Canadian Chronic Disease Surveillance System. https://www.canada.ca/en/public-health/services/publications/diseases-conditions/heart-disease-canada-fact-sheet.html.

3. Bentzon JF, Otsuka F, Virmani R, Falk E. Mechanisms of Plaque Formation and Rupture. *Circ Res*. 2014;114(12). doi:10.1161/CIRCRESAHA.114.302721

4. Jebari-Benslaiman S, Galicia-García U, Larrea-Sebal A, et al. Pathophysiology of Atherosclerosis. *Int J Mol Sci*. 2022;23(6). doi:10.3390/ijms23063346

5. Parthasarathy S, Raghavamenon A, Garelnabi MO, Santanam N. Oxidized Low-Density Lipoprotein. In: ; 2010. doi:10.1007/978-1-60327-029-8_24

6. Granger DN, Senchenkova E. *Inflammation and the Microcirculation*. Morgan & Claypool Life Sciences; 2010.

7. Wynn TA, Vannella KM. Macrophages in Tissue Repair, Regeneration, and Fibrosis. *Immunity*. 2016;44(3). doi:10.1016/j.immuni.2016.02.015

8. Chistiakov DA, Sobenin IA, Orekhov AN. Vascular Extracellular Matrix in Atherosclerosis. *Cardiol Rev*. 2013;21(6). doi:10.1097/CRD.0b013e31828c5ced

9. Johnson JL. Matrix metalloproteinases: influence on smooth muscle cells and atherosclerotic plaque stability. *Expert Rev Cardiovasc Ther*. 2007;5(2):265-282. doi:10.1586/14779072.5.2.265

10. Badimon L, Vilahur G. Thrombosis formation on atherosclerotic lesions and plaque rupture. *J Intern Med*. 2014;276(6). doi:10.1111/joim.12296

11. Palta S, Saroa R, Palta A. Overview of the coagulation system. *Indian J Anaesth*. 2014;58(5):515-523. doi:10.4103/0019-5049.144643

12. Nilsson IM. Coagulation and Fibrinolysis. *Scand J Gastroenterol*. 1987;22(sup137). doi:10.3109/00365528709089754

13. Smith SA, Travers RJ, Morrissey JH. How it all starts: Initiation of the clotting cascade. *Crit Rev Biochem Mol Biol*. 2015;50(4). doi:10.3109/10409238.2015.1050550

14. Jennewein C, Tran N, Paulus P, Ellinghaus P, Eble JA, Zacharowski K. Novel Aspects of Fibrin(ogen) Fragments during Inflammation. *Molecular Medicine*. 2011;17(5-6). doi:10.2119/molmed.2010.00146

15. Weisel JW, Litvinov RI. Mechanisms of fibrin polymerization and clinical implications. *Blood*. 2013;121(10). doi:10.1182/blood-2012-09-306639

16. Hoffman M, Monroe D. A Cell-based Model of Hemostasis. *Thromb Haemost*. 2001;85(06). doi:10.1055/s-0037-1615947

17. Juhan-Vague I, Collen D. On the role of coagulation and fibrinolysis in atherosclerosis. *Ann Epidemiol*. 1992;2(4). doi:10.1016/1047-2797(92)90092-5

18. Camaré C, Pucelle M, Nègre-Salvayre A, Salvayre R. Angiogenesis in the atherosclerotic plaque. *Redox Biol*. 2017;12. doi:10.1016/j.redox.2017.01.007

19. Marutsuka K, Hatakeyama K, Yamashita A, Asada Y. Role of Thrombogenic Factors in the Development of Atherosclerosis. *J Atheroscler Thromb*. 2005;12(1). doi:10.5551/jat.12.1

20. Wilcox JN, Smith KM, Schwartz SM, Gordon D. Localization of tissue factor in the normal vessel wall and in the atherosclerotic plaque. *Proceedings of the National Academy of Sciences*. 1989;86(8). doi:10.1073/pnas.86.8.2839

21. Borissoff JI, Spronk HMH, ten Cate H. The Hemostatic System as a Modulator of Atherosclerosis. *New England Journal of Medicine*. 2011;364(18). doi:10.1056/NEJMra1011670

22. Grover SP, Mackman N. Tissue Factor. *Arterioscler Thromb Vasc Biol*. 2018;38(4). doi:10.1161/ATVBAHA.117.309846

23. Jaberi N, Soleimani A, Pashirzad M, et al. Role of thrombin in the pathogenesis of atherosclerosis. *J Cell Biochem*. 2019;120(4). doi:10.1002/jcb.27771

24. Martorell L, Martínez-González J, Rodríguez C, Gentile M, Calvayrac O, Badimon L. Thrombin and protease-activated receptors (PARs) in atherothrombosis. *Thromb Haemost*. 2008;99(02). doi:10.1160/TH07-08-0481

25. Posma JJ, Grover SP, Hisada Y, et al. Roles of Coagulation Proteases and PARs (Protease-Activated Receptors) in Mouse Models of Inflammatory Diseases. *Arterioscler Thromb Vasc Biol*. 2019;39(1). doi:10.1161/ATVBAHA.118.311655

26. Lee CJ, Ansell JE. Direct thrombin inhibitors. *Br J Clin Pharmacol*. 2011;72(4). doi:10.1111/j.1365-2125.2011.03916.x

27. di Nisio M, Middeldorp S, Büller HR. Direct Thrombin Inhibitors. *New England Journal of Medicine*. 2005;353(10). doi:10.1056/NEJMra044440

28. Chen A, Stecker E, A. Warden B. Direct Oral Anticoagulant Use: A Practical Guide to Common Clinical Challenges. *J Am Heart Assoc*. 2020;9(13). doi:10.1161/JAHA.120.017559

29. Wienen W, Stassen JM, Priepke H, Ries UJ, Hauel N. In-vitro profile and ex-vivo anticoagulant activity of the direct thrombin inhibitor dabigatran and its orally active prodrug, dabigatran etexilate. *Thromb Haemost*. 2007;98(07). doi:10.1160/TH07-03-0183

30. van Ryn J, Goss A, Hauel N, et al. The Discovery of Dabigatran Etexilate. *Front Pharmacol*. 2013;4. doi:10.3389/fphar.2013.00012

31. Connolly SJ, Ezekowitz MD, Yusuf S, et al. Dabigatran versus Warfarin in Patients with Atrial Fibrillation. *New England Journal of Medicine*. 2009;361(12). doi:10.1056/NEJMoa0905561

32. Pingel S, Tiyerili V, Mueller J, Werner N, Nickenig G, Mueller C. Experimental research Thrombin inhibition by dabigatran attenuates atherosclerosis in ApoE deficient mice. *Archives of Medical Science*. 2014;1. doi:10.5114/aoms.2014.40742

33. Lee IO, Kratz MT, Schirmer SH, Baumhäkel M, Böhm M. The Effects of Direct Thrombin Inhibition with Dabigatran on Plaque Formation and Endothelial Function in Apolipoprotein E-Deficient Mice. *Journal of Pharmacology and Experimental Therapeutics*. 2012;343(2). doi:10.1124/jpet.112.194837

34. Preusch MR, Ieronimakis N, Wijelath ES, et al. Dabigatran etexilate retards the initiation and progression of atherosclerotic lesions and inhibits the expression of oncostatin M in apolipoprotein E-deficient mice. *Drug Des Devel Ther*. Published online September 2015. doi:10.2147/DDDT.S86969

35. Kadoglou NPE, Moustardas P, Katsimpoulas M, et al. The Beneficial Effects of a Direct Thrombin Inhibitor, Dabigatran Etexilate, on the Development and Stability of Atherosclerotic Lesions in Apolipoprotein E-deficient Mice. *Cardiovasc Drugs Ther*. 2012;26(5). doi:10.1007/s10557-012-6411-3

36. Villines TC, Ahmad A, Petrini M, et al. Comparative safety and effectiveness of dabigatran vs. rivaroxaban and apixaban in patients with non-valvular atrial fibrillation: a retrospective study from a large healthcare system. *Eur Heart J Cardiovasc Pharmacother*. 2019;5(2). doi:10.1093/ehjcvp/pvy044

37. Ezekowitz MD, Connolly S, Parekh A, et al. Rationale and design of RE-LY: Randomized evaluation of long-term anticoagulant therapy, warfarin, compared with dabigatran. *Am Heart J*. 2009;157(5). doi:10.1016/j.ahj.2009.02.005

38. Ezekowitz MD, Reilly PA, Nehmiz G, et al. Dabigatran With or Without Concomitant Aspirin Compared With Warfarin Alone in Patients With Nonvalvular Atrial Fibrillation (PETRO Study). *Am J Cardiol*. 2007;100(9). doi:10.1016/j.amjcard.2007.06.034

39. Franchi F, Rollini F, Cho JR, et al. Effects of dabigatran on the cellular and protein phase of coagulation in patients with coronary artery disease on dual antiplatelet therapy with aspirin and clopidogrel. *Thromb Haemost*. 2016;115(03). doi:10.1160/th15-06-0467

40. Arantes FBB, Menezes FR, Franci A, et al. Influence of Direct Thrombin Inhibitor and Low Molecular Weight Heparin on Platelet Function in Patients with Coronary Artery Disease: A Prospective Interventional Trial. *Adv Ther*. 2020;37(1). doi:10.1007/s12325-019-01153-8

41. Connolly SJ, Wallentin L, Ezekowitz MD, et al. The Long-Term Multicenter Observational Study of Dabigatran Treatment in Patients With Atrial Fibrillation (RELY-ABLE) Study. *Circulation*. 2013;128(3). doi:10.1161/CIRCULATIONAHA.112.001139

42. Emini Veseli B, Perrotta P, de Meyer GRA, et al. Animal models of atherosclerosis. *Eur J Pharmacol*. 2017;816. doi:10.1016/j.ejphar.2017.05.010

43. Getz GS, Reardon CA. Diet and Murine Atherosclerosis. *Arterioscler Thromb Vasc Biol*. 2006;26(2). doi:10.1161/01.ATV.0000201071.49029.17

44. Braun A, Trigatti BL, Post MJ, et al. Loss of SR-BI Expression Leads to the Early Onset of Occlusive Atherosclerotic Coronary Artery Disease, Spontaneous Myocardial Infarctions, Severe Cardiac Dysfunction, and Premature Death in Apolipoprotein E–Deficient Mice. *Circ Res*. 2002;90(3). doi:10.1161/hh0302.104462

45. Yu P, Xiong T, Tenedero CB, et al. Rosuvastatin Reduces Aortic Sinus and Coronary Artery Atherosclerosis in SR-B1 (Scavenger Receptor Class B Type 1)/ApoE (Apolipoprotein E) Double Knockout Mice Independently of Plasma Cholesterol Lowering. *Arterioscler Thromb Vasc Biol*. 2018;38(1). doi:10.1161/ATVBAHA.117.305140

46. Preusch MR, Ieronimakis N, Wijelath ES, et al. Dabigatran etexilate retards the initiation and progression of atherosclerotic lesions and inhibits the expression of oncostatin M in

apolipoprotein E-deficient mice. *Drug Des Devel Ther*. Published online September 2015. doi:10.2147/DDDT.S86969

47. Kadoglou NPE, Moustardas P, Katsimpoulas M, et al. The Beneficial Effects of a Direct Thrombin Inhibitor, Dabigatran Etexilate, on the Development and Stability of Atherosclerotic Lesions in Apolipoprotein E-deficient Mice. *Cardiovasc Drugs Ther*. 2012;26(5). doi:10.1007/s10557-012-6411-3

48. Canto I, J.K. Soh U, Trejo J. Allosteric Modulation of Protease-Activated Receptor Signaling. *Mini-Reviews in Medicinal Chemistry*. 2012;12(9). doi:10.2174/138955712800959116

49. Woźniak E, Broncel M, Bukowska B, Gorzelak-Pabiś P. The Protective Effect of Dabigatran and Rivaroxaban on DNA Oxidative Changes in a Model of Vascular Endothelial Damage with Oxidized Cholesterol. *Int J Mol Sci*. 2020;21(6). doi:10.3390/ijms21061953

50. Meh DA, Siebenlist KR, Mosesson MW. Identification and Characterization of the Thrombin Binding Sites on Fibrin. *Journal of Biological Chemistry*. 1996;271(38). doi:10.1074/jbc.271.38.23121

51. Lovely RS, Moaddel M, Farrell DH. Fibrinogen γ′ chain binds thrombin exosite II. *Journal of Thrombosis and Haemostasis*. 2003;1(1). doi:10.1046/j.1538-7836.2003.00027.x

52. Kawanami D, Matoba K, Kanazawa Y, Ishizawa S, Yokota T, Utsunomiya K. Thrombin induces MCP-1 expression through Rho-kinase and subsequent p38MAPK/NF-κB

signaling pathway activation in vascular endothelial cells. *Biochem Biophys Res Commun*. 2011;411(4). doi:10.1016/j.bbrc.2011.07.031

53. Dólleman SC, Agten SM, Spronk HMH, et al. Thrombin in complex with dabigatran can still interact with PAR-1 via exosite-I and instigate loss of vascular integrity. *Journal of Thrombosis and Haemostasis*. 2022;20(4). doi:10.1111/jth.15642

54. Achilles A, Mohring A, Dannenberg L, et al. Dabigatran enhances platelet reactivity and platelet thrombin receptor expression in patients with atrial fibrillation. *Journal of Thrombosis and Haemostasis*. 2017;15(3). doi:10.1111/jth.13595

55. Pawlinski R, Tencati M, Hampton CR, et al. Protease-Activated Receptor-1 Contributes to Cardiac Remodeling and Hypertrophy. *Circulation*. 2007;116(20). doi:10.1161/CIRCULATIONAHA.107.692764

56. Sabri A, Short J, Guo J, Steinberg SF. Protease-Activated Receptor-1–Mediated DNA Synthesis in Cardiac Fibroblast Is via Epidermal Growth Factor Receptor Transactivation. *Circ Res*. 2002;91(6). doi:10.1161/01.RES.0000035242.96310.45